[logo=uiologo-45mm,subtitle=Shell structures around A = 16,date=June 2008]

Contents

Chapter 1

Introduction

The purpose of this thesis was to see if nuclear many-body theory could predict the unexpectedly low experimental value of the $E(2_1^+)$ excitation strength for ^{16}C. This value was reported by Imai et al. [1]. They measured an unexpectedly low E2 transition strength between the first 2_1^+ and 0^+ states of ^{16}C. The measured value was $0.63e^2\text{fm}^4$.

This result came as a surprise because the reduced electric quadrupole (E2) transition probability B(E2) between the first 2_1^+ and 0^+ state is proportional to the inverse of the excitation energy of the 2_1^+ state $E(2_1^+)$. This implies that the B(E2) should be low at the beginning or end of a closed shell, and high in the middle of a shell. For ^{14}C the excitation energy is 7.01 MeV and the transition strength is $3.7e^2\text{fm}^4$. Since the excitation energy for ^{16}C is 1.77 MeV, one would expect the transition strength to increase. However, the measured transition strength of $0.63e^2\text{fm}^4$ was much lower than the $E(2_1^+)$ transition for ^{14}C.

This experiment led to speculations that some new physics might be involved in ^{16}C. To understand this experiment and the low-lying structure of ^{16}C, possible proton-neutron correlations were discussed, in contrast to the accepted picture which said that these low-lying states were ruled mainly by neutron excitations.

The experimental results of [1] lead different experimental groups to remeasure this transition. The transition strength of ^{16}C has recently been measured by several groups, such as Wiedeking et al. [2]. Their new experimental value is 4.15fm^4, in accordance with theoretical predictions.

The aim of this thesis is to calculate this transition strength of ^{16}C and study the structure of nuclei near ^{16}C in order to understand the degrees of freedom involved in the low-lying states of these nuclei.The main emphasis, in addition to the structure of ^{16}C and the above transition, is to study the energy spectra for ^{14}C, ^{16}C, ^{15}B and, if time permits, ^{15}C. I will do shell-model calculations using existing codes for shell-model and effective interaction calculations developed in Oslo. All codes are available at http://www.fys.uio.no/compphys.

Finding the energy spectra is interesting because the nucleon-nucleon (NN) interaction is not known in closed form like the Coulomb interaction. To calculate it

accurately one would have to go to Quantum Chromo Dynamics and look at the interaction between the quarks making up the nucleons, but this is at present impossible to calculate accurately. Furthermore the nucleons form a many-particle problem that can only be solved approximately. It is therefore important to get more data on how our theoretical models correspond with the experimental data, so we can achieve a better understanding of the NN interaction in the medium.

The program I will use finds the energy for the ground state and a given number of excited states, for a given nucleus in a given model space. The program works in three steps. First it renormalizes the NN interaction. Then it finds an effective interaction using many-body perturbation theoy. These calculations depend on the chosen model space. This model space is chosen according to the relevant degrees of freedom of a specific nucleus. Finally it finds the energy eigenvalues of the Hamiltonian by calculating two-body interactions in the shell-model.

One of the larger problems in nuclear physics is finding good single particle (sp) energies that accurately predict the energy spectrum. These are usually free parameters that are adjusted to fit the experimental data. I will try out two different sets of single particle energies. The program I use calculates the single particle energies when it finds the effective interaction. I will use both these single-particle energies and the single particle energies that E. K. Warburton and B. A. Brown give for ^{16}O in Ref. [3]. The single-particle energies derived from ^{16}O are expected to be close to the single-particle energies for ^{16}C.

There have been few calculations in large model spaces such as the ones I will look at. It will be interesting to see if using such large model spaces can predict the experimental values without having to adjust the effective interaction to each nucleus. There have also been few calculations that mix the $0p$ and $1s0d$ shells, as these calculations have been difficult to do. Such large calculations are, however, now possible due to better algorithms and the advancement of computation power.

The reason I look at the nuclei ^{14}C, ^{15}B and ^{15}C in addition to ^{16}C, is that their structure is close to ^{16}C (see figures 1.1, 1.2, 1.3, 1.4). The particles in a nucleus have a higher probability to excite to another orbital within the same shell (f.ex. $0d_{\frac{5}{2}}$ to $1s_{\frac{1}{2}}$) than exciting to an orbital in another shell (f.ex. $0p_{\frac{1}{2}}$, $0d_{\frac{5}{2}}$). The protons in ^{16}C fills the $0p_{\frac{3}{2}}$ orbital, and the nucleus has two neutrons outside the filled $0p$ shell. We can then expect that the number of neutrons in the $0p$ shell will not change much when we go from the ground state to higher-lying excited states. The neutrons in the $1s0d$ shell however, will have a high excitation probability. The protons in ^{16}C will mainly excite to the $0p_{\frac{1}{2}}$ orbital, and should also be lower than the neutron excitation, as they fill an orbital. ^{15}B and ^{16}C have the same number of neutrons. The neutron excitations of ^{15}B should therefore be similar to the neutron excitations of ^{16}C. ^{15}C and ^{16}C should have similar proton excitations.

Ideally one should use the full Hilbert space when calculating the energy spectrum. Since the Hilbert space is infinitely large, this is impossible. I will therefore use a reduced model space, such as the one given in figures 1.1, 1.2, 1.3 and 1.4. The higher-lying shells should give less and less contribution to the energy of the nucleus, as the particles need more energy to excite up to them. I will, because of this and because

the size of the Hamiltonian matrix quickly explodes for a large number of orbitals, use only the 0s0p and $1s0d$ shells as my model space. More specifically, I will use the orbitals $0p_{\frac{3}{2}}$, $0p_{\frac{1}{2}}$, $0d_{\frac{5}{2}}$, $1s_{\frac{1}{2}}$ and $0p_{\frac{3}{2}}$, $0p_{\frac{1}{2}}$, $0d_{\frac{5}{2}}$, $1s_{\frac{1}{2}}$, $0d_{\frac{3}{2}}$ as my model spaces. The $0p_{\frac{3}{2}}$ - $1s_{\frac{1}{2}}$ and $0p_{\frac{3}{2}}$ - $0d_{\frac{3}{2}}$ model spaces will hopefully show a convergence of energy. If not I should include the next orbital, namely the $0f_{\frac{7}{2}}$ orbital. However, this model space will probably be too big, as the number of possible sp states for ^{16}C increases by a factor of 35. Also I expect the contribution from the $0f_{\frac{7}{2}}$ orbital to be very low, as it is in a new shell, with a high energy gap between it and the $0d_{\frac{3}{2}}$ orbital.

With convergence, I mean that the energy values we get from the program will not change when we increase our model space. This will imply that increasing our model space further will not significantly change the energy values we get.

The energy spectra for ^{14}C, ^{16}C, ^{15}B and ^{15}C will be calculated using four different approaches to the effective interaction, based on many-body perturbation theory to third order [4]. These four approaches employ as starting points a G-matrix with a harmonic-oscillator basis, a G-matrix with a Hartree-Fock basis, a renormalized NN interaction based on the Vlowk method [5] and a harmonic oscillator basis, and finally a Vlowk interaction with a Hartree-Fock basis. I will in the final chapter discuss which of these methods are best, and choose that method to represent our findings.

In the next two chapters we will discuss how the shell model program works.

In chapter 2 we discuss the renormalization of the Hamiltonian by approximating the many-body interaction to a two-particle interaction working in our model space. We also discuss the Hartree-Fock method.

In chapter 3 we show how we numerically solve our Hamiltonian in the m-scheme through an iterative numerical method known as the Lanczos algorithm. We also discuss some of the theory for electromagnetic transitions in the nuclei.

In the chapter 4 we discuss the results we have gotten from our calculations.

Our conclusions are presented in the last chapter.

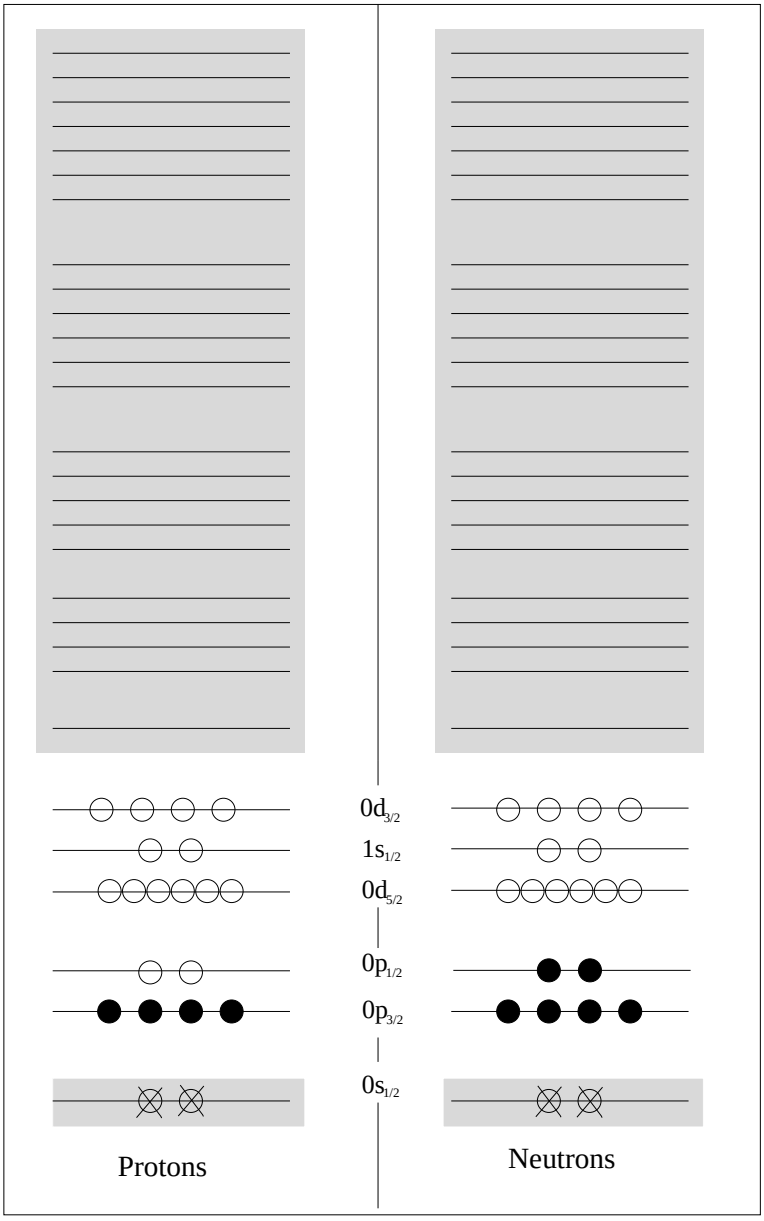

Figure 1.1: Model-space for ^{14}C. Filled circles represent nucleons that are free to be excited. The circles with a cross over them represent nucleons that are held still in their respective orbitals, and are not allowed to be excited. The empty circles represent available states that the nucleons can be excited to. The gray box indicates the excluded states that form the effective interaction.

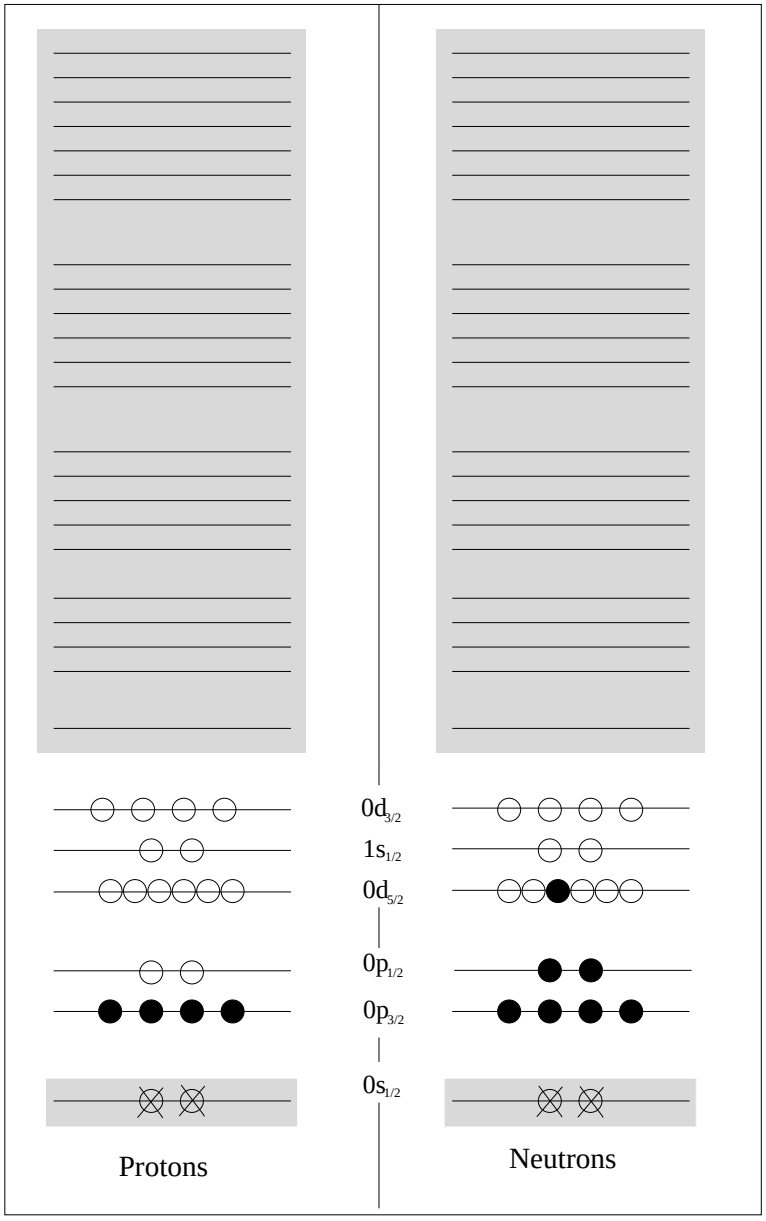

Figure 1.2: Model-space for ^{15}C. Filled circles represent nucleons that are free to be excited. The circles with a cross over them represent nucleons that are held still in their respective orbitals, and are not allowed to be excited. The empty circles represent available states that the nucleons can be excited to. The gray box indicates the excluded states that form the effective interaction.

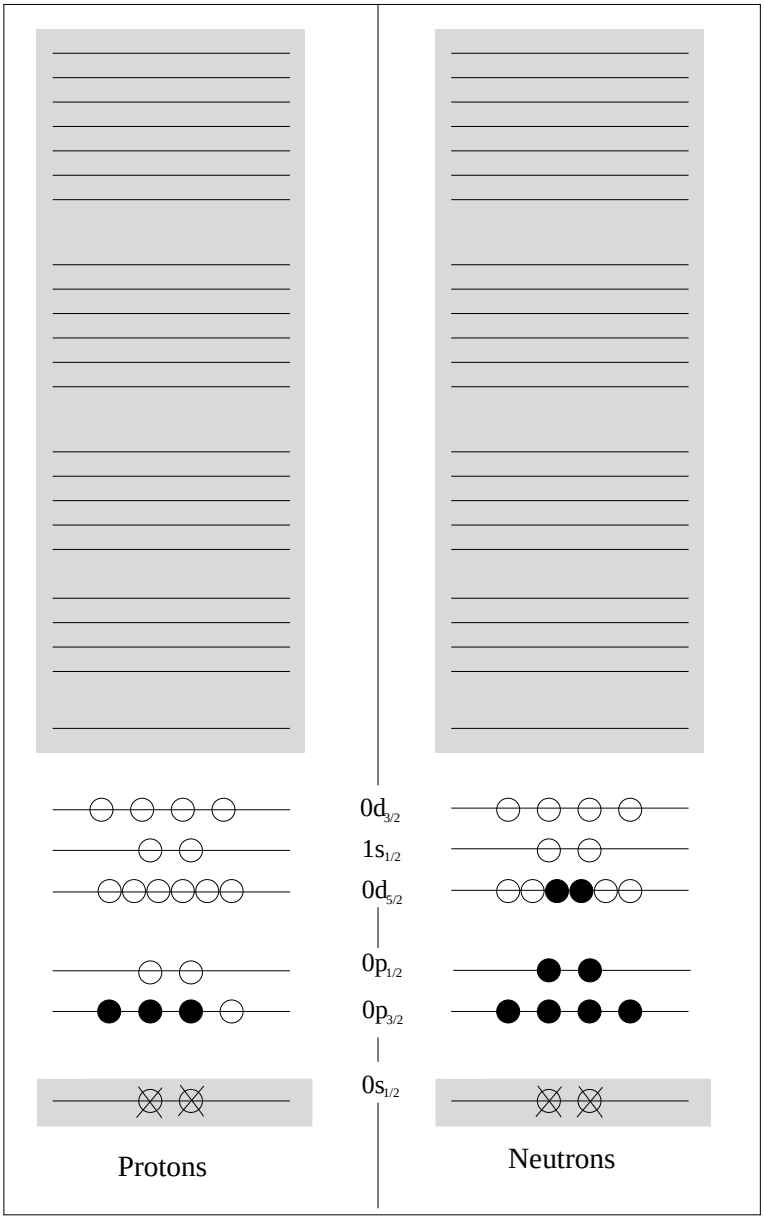

Figure 1.3: Model-space for ^{15}B. Filled circles represent nucleons that are free to be excited. The circles with a cross over them represent nucleons that are held still in their respective orbitals, and are not allowed to be excited. The empty circles represent available states that the nucleons can be excited to. The gray box indicates the excluded states that form the effective interaction.

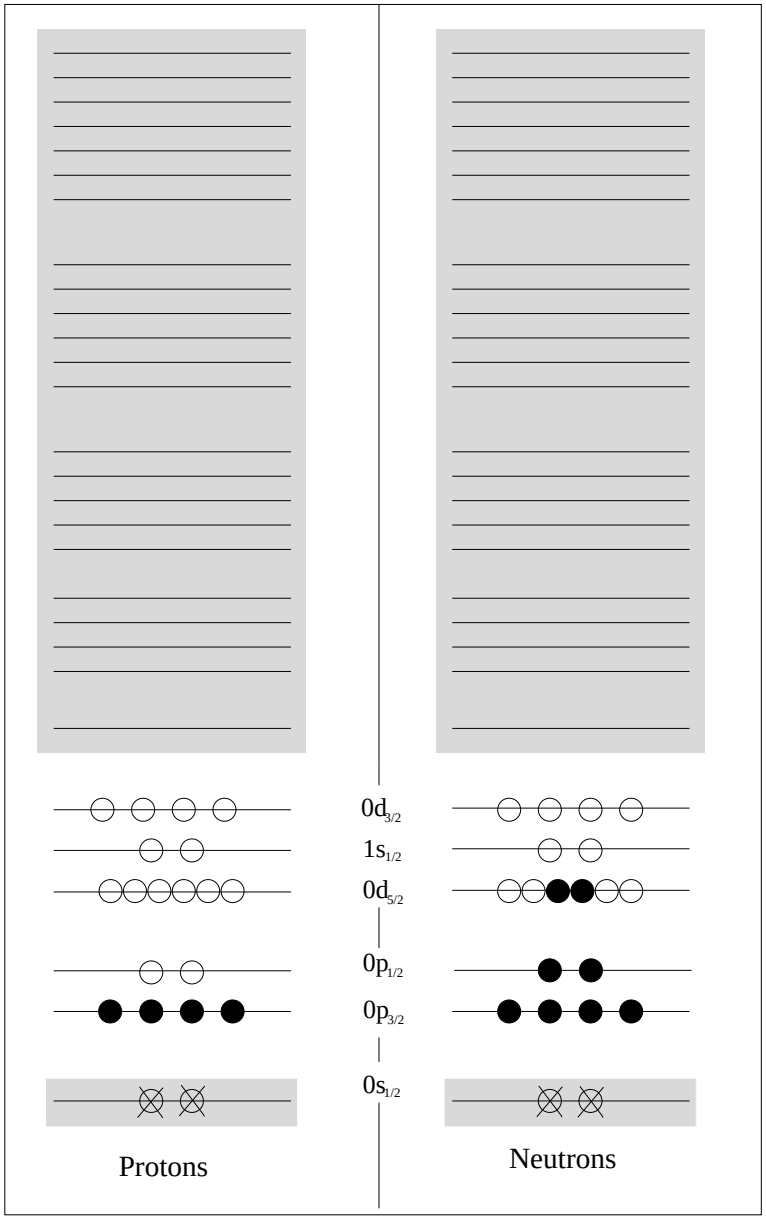

Figure 1.4: Model-space for ^{16}C. Filled circles represent nucleons that are free to be excited. The circles with a cross over them represent nucleons that are held still in their respective orbitals, and are not allowed to be excited. The empty circles represent available states that the nucleons can be excited to. The gray box indicates the excluded states that form the effective interaction.

Chapter 2

Renormalizing the Hamiltonian

The calculations done in this thesis are based on the framework of the nuclear shell model, with neutrons and protons as degrees of freedom. The effective interactions are based on a renormalized nucleon-nucleon (NN) interaction including the Coulomb force.

The renormalization of the Hamiltonian is done in a harmonic oscillator basis. This basis is also used for the Hartree-Fock calculations.

2.1 Renormalizing the Hamiltonian

We want to solve the non-relativistic Shcrödinger equation for the nuclei ^{14}C, ^{16}C, ^{15}B and ^{15}C,

$$\hat{H}\left|\Psi(1\ldots A)\right\rangle = E\left|\Psi(1\ldots A)\right\rangle. \tag{2.1}$$

Equation 2.1 is a many-particle equation that must be solved approximately. Here we will approximate it by using two-particle interactions. This is because the three-particle and higher interactions are more difficult to calculate, and give smaller contributions to the total interaction. Note that three-particle interactions can have a significant impact on the binding energy, providing up to 10% of the total energy, and sometimes influencing the energy spectra.

The two-body Hamiltonian is given by

$$\hat{H} = \hat{T} + \hat{V} = \sum_{i=1}^{A} \hat{t}_i + \sum_{i<j} \hat{V}_{ij}, \tag{2.2}$$

where $\hat{t}_i$ is the kinetic energy of nucleon i and $\hat{V}_{ij}$ is the nucleon nucleon (NN) interaction between particle i and j. In nuclear physics the NN interaction V is not well known, and there exists many methods to derive it.

This Hamiltonian is often rewritten using an auxiliary potential $\hat{U}$,

$$\hat{H} = (\hat{T} + \hat{U}) + (\hat{V} - \hat{U}) = \hat{H}_0 + \hat{H}_1, \tag{2.3}$$

where we want to choose $\hat{U}$ so that $\hat{H}_1$ is small.

Our two-body Hamiltonian consists of A nucleons interacting with each other in our infinite Hilbert space, and is too large for practical calculations. We will use ^{4}He as a closed core to reduce this space. This means that the four first nucleons of our nuclei cannot be excited to higher-lying states. ^{4}He fills the $0s$ shell, and is very stable. Excitations from the $0s$ shell is therefore highly unlikely, and using it as a closed core will be a good approximation. The closed core will be our new reference vacuum.

The nucleus ^{4}He is

$$|c\rangle = \prod_{i=1}^{4} a_i^\dagger |0\rangle . \tag{2.4}$$

We will also map our Hamiltonian down on a reduced Hilbert space, our so-called model space.

The wave function $|\Psi_\lambda\rangle$ in the full Hilbert space is

$$|\Psi_\lambda\rangle = \sum_{\lambda=1}^{\infty} b_\lambda |\phi_\lambda\rangle . \tag{2.5}$$

We divide the Hilbert space into a model space and an excluded state with the projection operators $\hat{P}$ and $\hat{Q}$, that map the full Hilbert space to respectively the model space and the excluded space,

$$\hat{P} = \sum_{i=1}^{d} |\phi_i\rangle \langle\phi_i| , \tag{2.6}$$

$$\hat{Q} = \sum_{i=d+1}^{\infty} |\phi_i\rangle \langle\phi_i| , \tag{2.7}$$

d is here the dimensionality of the model space.

The projection operators $\hat{P}$ and $\hat{Q}$ are hermitian, and fulfill the relations $\hat{P}\hat{Q} = 0$, $\hat{P}^2 = \hat{P}$, $\hat{Q}^2 = \hat{Q}$ and $\hat{P} + \hat{Q} = 1$.

In our calculations we will work with three different model spaces. These model spaces are listed below.

- I now define the shorthand notation $0p\frac{3}{2} - 1s\frac{1}{2}$. This notation comprises the following single particle orbitals, $0p\frac{3}{2}$, $0p\frac{1}{2}$, $0d\frac{5}{2}$ and $1s\frac{1}{2}$ for neutrons and protons. The notation $0p\frac{3}{2} - 1s\frac{1}{2}$ will hereafter be used for this model space.

- I now define the shorthand notation $0p\frac{3}{2} - 0d\frac{3}{2}$. This notation comprises the following single particle orbitals, $0p\frac{3}{2}$, $0p\frac{1}{2}$, $0d\frac{5}{2}$, $1s\frac{1}{2}$ and $0d\frac{3}{2}$ for neutrons and protons. The notation $0p\frac{3}{2} - 0d\frac{3}{2}$ will hereafter be used for this model space.

- I now define the shorthand notation $0p\frac{3}{2} - 0f\frac{7}{2}$. This notation comprises the following single particle orbitals, $0p\frac{3}{2}$, $0p\frac{1}{2}$, $0d\frac{5}{2}$ $1s\frac{1}{2}$, $0d\frac{3}{2}$ and $0f\frac{7}{2}$ for neutrons and protons. The notation $0p\frac{3}{2} - 0f\frac{7}{2}$ will hereafter be used for this model space.

Using the $\hat{P}$ and $\hat{Q}$ projection operators one can derive a new two-body interaction that is effective only in the model space. This $\hat{V}_{\text{eff}}$ is also known as the $\hat{\hat{Q}}$-box,

$$\hat{V}_{\text{eff}}(\omega) = \hat{\hat{Q}}(\omega) = \hat{P}(\hat{H}_1 + \hat{H}_1 \frac{\hat{Q}}{\omega - \hat{H}_0 - \hat{Q}\hat{H}_1\hat{Q}} \hat{Q}\hat{H}_1)\hat{P} \tag{2.8}$$

$$= \hat{P}(\hat{H}_1 + \hat{H}_1 \frac{\hat{Q}}{\omega - \hat{H}_0}\hat{H}_1 + \hat{H}_1 \frac{\hat{Q}}{\omega - \hat{H}_0}\hat{H}_1 \frac{\hat{Q}}{\omega - \hat{H}_0}\hat{H}_1 + \dots)\hat{P}, \tag{2.9}$$

where ω is a general energy variable, the so-called starting energy. See [6] for more details. This equation is also known as the Rayleigh-Schrödinger perturbative expansion.

For simplicity we will write $\hat{H}_1$ as $\hat{V}$ in our equations.

The $\hat{\hat{Q}}$-box can thus be expanded in a diagrammatic expansion of the NN interaction, as shown in figure 2.1. Note that in this case the model space is defined by the hole states. Figure 2.1 i) shows a closed, first order Goldstone diagram, while diagram ii) shows a closed, second order Goldstone diagram and diagram iii) shows a closed, third order Goldstone diagram.

Diagram i) can be expressed as

$$(i) = \frac{(-)^{n_h+n_l}}{2^{n_{ep}}} \sum_{k_i,k_j \leq k_F} \langle k_i k_j | \hat{\hat{V}} | k_i k_j \rangle_{AS}\,, \tag{2.10}$$

where n_h denotes the number of hole lines, n_l the number of closed fermion loops and n_{ep} is the number of equivalent pairs. The subscript AS denotes the antisymmetrized and normalized matrix element

$$\langle k_i k_j | \hat{\hat{V}} | k_i k_j \rangle_{AS} = \langle k_i k_j | \hat{V} | k_i k_j \rangle - \langle k_j k_i | \hat{V} | k_i k_j \rangle = \hat{\hat{V}}_{ijij}. \tag{2.11}$$

Diagram (i) then becomes

$$(i) = \frac{(-)^{2+2}}{2^1} \sum_{ij \leq k_F} \hat{\hat{V}}_{ijij}. \tag{2.13}$$

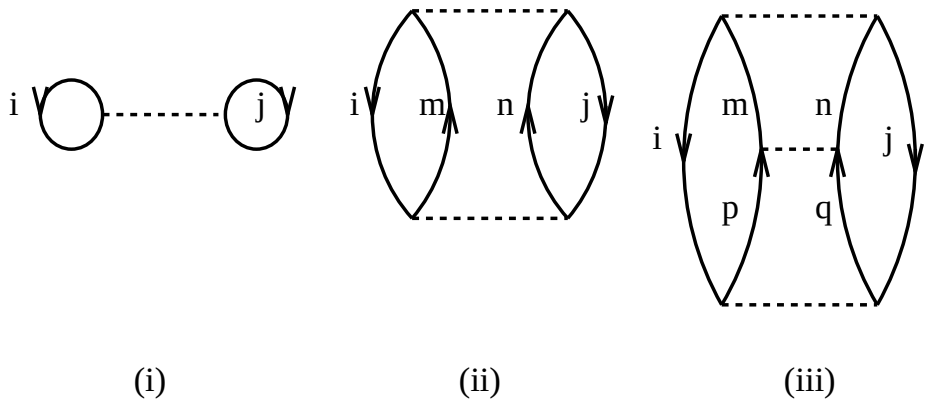

(2.12)

Figure 2.1: Closed Goldstone diagrams. Diagrams (i), (ii) and (iii) are, respectively, the first, second and third order contributions to the interaction $\hat{V}$.

Diagrams (ii) and (iii) gives

$$(ii) = \frac{(-)^{2+2}}{2^2} \sum_{ij \leq k_F} \sum_{mn > k_F} \frac{\hat{\tilde{V}}_{ijmn} \tilde{V}_{mnij}}{\varepsilon_i + \varepsilon_j - \varepsilon_m - \varepsilon_n}, \tag{2.14}$$

and

$$(iii) = \frac{(-)^{2+2}}{2^3} \sum_{ij \leq k_F} \sum_{mn > k_F} \sum_{pq > k_F} \frac{\hat{\tilde{V}}_{ijmn} \hat{\tilde{V}}_{mnpq} \hat{\tilde{V}}_{pqij}}{(\varepsilon_i + \varepsilon_j - \varepsilon_m - \varepsilon_n)(\varepsilon_i + \varepsilon_j - \varepsilon_p - \varepsilon_q)}. \tag{2.15}$$

Figure 2.2 shows that the interaction $\hat{V}$ is large for small values of the interparticle distance $\mathbf{r}$. We see readily from this and equation (2.15) that the Goldstone linked-diagram theory is unsuited for perturbation theory as the terms will only get larger when $\mathbf{r}$ is small.

We need to use another method to solve the Schrödinger equation. Two such methods that the program uses for finding the effective interaction are the G-matrix and the Vlowk methods.

2.2 G-matrix method

The G-matrix method was originally developed by Brueckner [7], and was further developed by Goldstone [8] and Bethe, Brandow and Petschek [9], see Ref. [4] for a historical overview. It involves the summation of all particle-particle ladder type of diagrams to inifnite order and serves therefore to renormalize the short-range part of the nucleon-nucleon interaction. See for Ref. [4] for more details. It can be written as

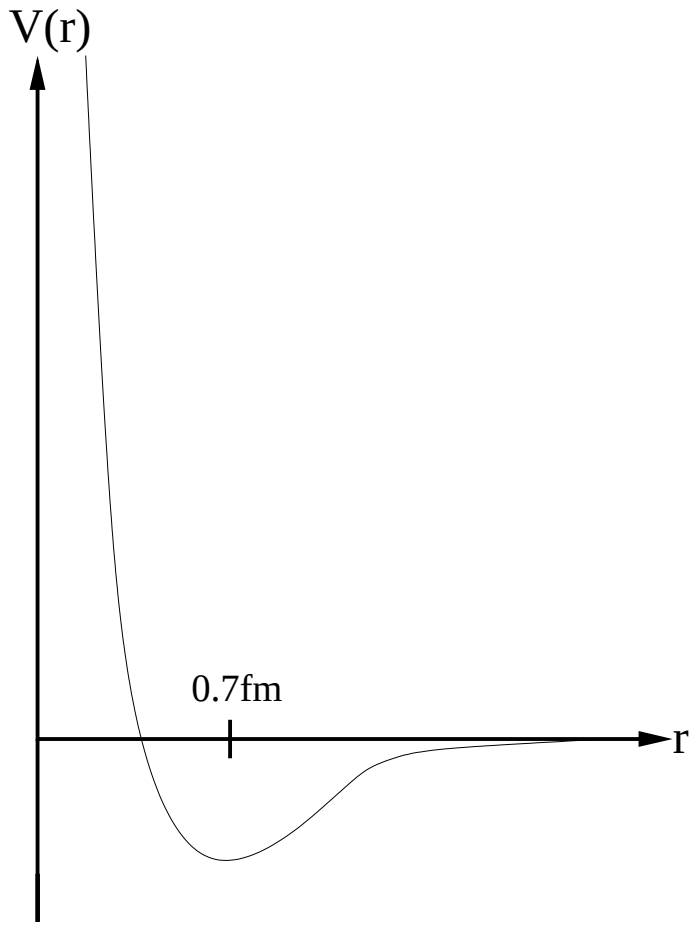

(2.16)

Figure 2.2: Schematic model for the NN potential.

$$\begin{aligned}\hat{\hat{G}}_{ijij} =& \frac{1}{2}\hat{\hat{V}}_{ijij} + \frac{1}{2}\sum_{mn>k_F}\frac{\hat{\hat{V}}_{ijmn}}{\varepsilon_i+\varepsilon_j-\varepsilon_m-\varepsilon_n} \\ &\times\left(\frac{1}{2}\hat{\hat{V}}_{mnij} + \frac{1}{2}\sum_{mn>k_F}\sum_{pq>k_F}\frac{\hat{\hat{V}}_{mnpq}}{\varepsilon_i+\varepsilon_j-\varepsilon_p-\varepsilon_q}\right) \\ &\times\left(\frac{1}{2}\hat{\hat{V}}_{pqij}+\dots\right). \end{aligned} \tag{2.17}$$

This is a recursive equation, and can thus be written as

$$\hat{\hat{V}}_{ijij} = \frac{1}{2}\hat{\hat{V}}_{ijij} + \frac{1}{2}\sum_{mn>k_F}\hat{\hat{V}}_{ijmn}\frac{1}{\varepsilon_i+\varepsilon_j-\varepsilon_m-\varepsilon_n}\hat{\hat{G}}_{mnij}. \tag{2.18}$$

Although the interaction diverges for small values of $\mathbf{r}$ and although we have an infinite sum, we know that the energy of the system is still finite. This means that the sum in equation 2.18 is convergent and can therefore be calculated accurately.

The single particle (sp) energies ε are given by the unperturbed (non-interacting) Hamiltonian $\hat{H}_0$

$$\hat{H}_0\left|\psi_m\psi_n\right\rangle = (\varepsilon_m+\varepsilon_n)\left|\psi_m\psi_n\right\rangle. \tag{2.19}$$

We can now, using the projection operator $\hat{Q}$ defined in equation 2.7, rewrite the G-matrix into a more general form

$$\hat{G}(\omega) = \hat{V} + \hat{V}\frac{\hat{Q}}{\omega-\hat{H}_0}\hat{G}(\omega), \tag{2.20}$$

where ω is a general energy variable, that is, the unperturbed sp energies for a general two-particle state.

Equation 2.20 assumes that $\hat{H}_0$ commutes with $\hat{Q}$. If this is not the case, then the G-matrix assumes the form

$$\hat{G}(\omega) = \hat{V} + \hat{V}\hat{Q}\frac{1}{\omega-\hat{Q}\hat{H}_0\hat{Q}}\hat{Q}\hat{G}(\omega). \tag{2.21}$$

We will in our coming calculations assume that $\hat{H}_0$ commutes with $\hat{Q}$. This is safe to do because we can always choose $\hat{U}$ so that $\hat{H}_0$ will commute with $\hat{Q}$.

Equation 2.20 is still problematic though, as we have the infinitely large excluded space in it. To solve this we introduce a free scattering interaction matrix ($\hat{G}_F$, which is easy to calculate), in order to get rid of the excluded space dependency. In order to do this we need to define two matrices $\hat{G}$ and $\hat{G}_F$, where $\hat{G}$ is the effective two-body interaction for bound states, and $\hat{G}_F$ is the free G-matrix, that is, the free scattering

two-body interaction. I will, for simplicity, from now on write $\hat{G}(\omega)$ as $\hat{G}$.

Before I define the G_F-matrix, I will show how we can express one G-matrix by another G-matrix, see Ref. [4] for more details.

We define two G-matrices,

$$\hat{G}_1 = \hat{V}_1 + \hat{V}_1 \frac{\hat{Q}_1}{\hat{e}_1} \hat{G}_1, \tag{2.22}$$

$$\hat{G}_2 = \hat{V}_2 + \hat{V}_2 \frac{\hat{Q}_2}{\hat{e}_2} \hat{G}_2, \tag{2.23}$$

where

$$\hat{e}_i = \omega_i - \hat{Q}_i \hat{H}_0 \hat{Q}_i, \qquad i = 1, 2.$$

We define the wave operators

$$\hat{\Omega}_i = 1 + \frac{\hat{Q}_i}{\hat{e}_i} \hat{G}_i, \qquad i = 1, 2 \tag{2.24}$$

This leads to the following relation

$$\hat{G}_i = \hat{V}_i \hat{\Omega}_i, \qquad i = 1, 2. \tag{2.25}$$

We can now write $\hat{G}_1$ as

$$\hat{G}_1 = \hat{G}_1 - \hat{G}_2^\dagger \left(\hat{\Omega}_1 - 1 - \frac{\hat{Q}_1}{\hat{e}_1} \hat{G}_1 \right) + \left(\hat{\Omega}_2^\dagger - 1 - \hat{G}_2^\dagger \frac{\hat{Q}_2}{\hat{e}_2} \right) \hat{G}_1, \tag{2.26}$$

and using equation 2.25 we get

$$\hat{G}_1 = \hat{G}_2^\dagger + \hat{G}_2^\dagger \left(\frac{\hat{Q}_1}{\hat{e}_1} - \frac{\hat{Q}_2}{\hat{e}_2} \right) \hat{G}_1 + \hat{\Omega}_2^\dagger (\hat{V}_1 - \hat{V}_2) \hat{\Omega}_1. \tag{2.27}$$

When $\hat{V}_1 = \hat{V}_2$ equation 2.27 reduces to

$$\hat{G}_1 = \hat{G}_2^\dagger + \hat{G}_2^\dagger \left(\frac{\hat{Q}_1}{\hat{e}_1} - \frac{\hat{Q}_2}{\hat{e}_2} \right) \hat{G}_1. \tag{2.28}$$

Now we can go back to the free G-matrix. The G_F-matrix is basis-independent, and is defined as

$$\hat{G}_F = \hat{V} + \hat{V} \frac{1}{\tilde{\omega} - T} \hat{G}_F, \tag{2.29}$$

where $\hat{V}$ is the usual two-body interaction, T is the kinetic term and ω is the unperturbed energy.

Since $\hat{G}$ and $\hat{G}_F$ have the same NN interaction, we can use equation 2.28 to define

$\hat{G}$,

$$\hat{G} = \hat{G}_F^\dagger + \hat{G}_F^\dagger \left(\frac{\hat{Q}}{\hat{e}} - \frac{1}{\hat{e}_F} \right) \hat{G}, \tag{2.30}$$

where we have used the fact that $\hat{Q}_F = 1$.

Using the matrix relation

$$\hat{Q}\frac{1}{\hat{Q}\hat{e}\hat{Q}}\hat{Q} = \frac{1}{\hat{e}} - \frac{1}{\hat{e}}\hat{P}\frac{1}{\hat{P}\frac{1}{\hat{e}}\hat{P}}\hat{P}\frac{1}{\hat{e}}, \tag{2.31}$$

we can rewrite equation 2.21 as

$$\hat{G} = \hat{G}_F + \Delta\hat{G}, \tag{2.32}$$

where $\Delta\hat{G}$ is a correction term, defined fully in the model space P, that gives us the bound energies. It is given as

$$\Delta\hat{G} = -\hat{G}_F\frac{1}{\hat{e}}\hat{P}\frac{1}{\hat{P}\left(\frac{1}{\hat{e}} + \frac{1}{\hat{e}}\hat{G}_f\frac{1}{\hat{e}}\right)\hat{P}}\hat{P}\frac{1}{\hat{e}}\hat{G}_F. \tag{2.33}$$

The $\Delta\hat{G}$ matrix is expressed in terms of the free interaction matrix G_F, and is not dependent on the high-lying states in the excluded space Q. The G_F matrix can be calculated numerically exactly for the full two-particle Hilbert space, and this makes the $\Delta\hat{G}$ matrix easy to calculate.

Note that the G_F matrix is still a recursive equation that needs to be solved.

2.3 Vlowk method

The Vlowk method renormalizes the Hamiltonian in the momentum space. First we use a similarity transformation of the full Hilbert space to the momentum space. This transformation is numerically exact. In the momentum space basis we introduce a cutoff, were we exclude the states with high momenta. This cutoff is necessary because we do not have a one to one correspondence when going from the full momentum space. The low-momentum space will then be part of our model space P, while the high momentum space will be part of our excluded state Q. The NN interaction is strongly dependent upon this cutoff, so care must be taken when choosing where to set the cutoff. Due to the choice of cutoff, this introduces a stronger dependency on many-body forces than the G-matrix. We need at least three-body forces computed with the same cutoff.

We have chosen a cutoff of 2.2 fm^{-1} in our calculations.

We start by using the Lee and Suzuki similarity transformation of the full two-

particle Hamiltonian,

$$\hat{\mathscr{H}} = \hat{X}^{-1}\hat{H}\hat{X}. \tag{2.34}$$

We divide the Hilbert space into the P and Q spaces. For the Vlowk method these P and Q spaces are not the same as the models space given in figures 1.1-1.4. They are defined by the cutoff in momentum space mentioned above.

$$\hat{\mathscr{H}} = \begin{pmatrix} \hat{P}\hat{\mathscr{H}}\hat{P} & \hat{P}\hat{\mathscr{H}}\hat{Q} \\ \hat{Q}\hat{\mathscr{H}}\hat{P} & \hat{Q}\hat{\mathscr{H}}\hat{Q} \end{pmatrix} \tag{2.35}$$

The Lee and Suzuki iterative method involves choosing $\hat{X}$ as

$$\hat{X} = e^{\hat{w}}, \tag{2.36}$$

where $\hat{w}$, not to be confused with ω used in the previous section, is defined to have the relation

$$\hat{w} = \hat{Q}\hat{w}\hat{P}. \tag{2.37}$$

Using this definition of $\hat{w}$, $\hat{X}$ has the properties $\hat{X} = 1 + \hat{w}$ and $\hat{X}^{-1} = 1 - \hat{w}$.

When we require $\hat{\mathscr{H}}$ (2.35) to be block diagonal and set in for $\hat{X}$, we get

$$\hat{Q}\hat{\mathscr{H}}\hat{P} = \hat{Q}\hat{H}\hat{P} - \hat{w}\hat{H}\hat{P} + \hat{Q}\hat{H}\hat{w} - \hat{w}\hat{H}\hat{w} = 0. \tag{2.38}$$

We then need to solve this non-linear equation for $\hat{w}$.

When $\hat{w}$ is found, the Hamiltonian projected down on the model space $\hat{P}\hat{\mathscr{H}}\hat{P}$ becomes

$$\hat{H}_{\text{eff}} = \hat{P}\hat{H}\hat{P} + \hat{P}\hat{H}\hat{w} = \hat{P}\hat{H}\hat{P} + \hat{P}\hat{V}\hat{w}. \tag{2.39}$$

We now do another similarity transformation $\hat{U}$ on $\hat{H}_{\text{eff}}$ [10].

$$\hat{U} = (1 + \hat{w} - \hat{w}^\dagger)(1 + \hat{w}\hat{w}^\dagger + \hat{w}^\dagger\hat{w})^{-\frac{1}{2}} \tag{2.40}$$

We want the transformed Hamiltonian to be diagonal so that we can easily separate the interaction term from the kinetic term.

$$\hat{\tilde{V}} = \hat{U}^{-1}(\hat{H}_0 + \hat{V})\hat{U} - \hat{H}_0 \tag{2.41}$$

Using equations 2.39, 2.40 and 2.41 the effective interaction in the model space becomes

$$\hat{V}_{\text{eff}} = (\hat{P} + \hat{w}^\dagger\hat{w})^{\frac{1}{2}}(\hat{P}\hat{H}\hat{P} + \hat{P}\hat{V}\hat{w})(\hat{P} + \hat{w}^\dagger\hat{w})^{-\frac{1}{2}} - \hat{P}\hat{H}_0\hat{P}. \tag{2.42}$$

To solve this equation we need to calculate the matrix $(\hat{P} + \hat{w}^\dagger\hat{w})^{\frac{1}{2}}$, where $\hat{w}$ is found

through equation 2.38.

I will now very shortly mention how to transform to the momentum space. For further details, see [5].

We start by solving the Schrödinger equation in relative momentum space

$$\int dk' k'^2 \langle k| T + V \left|k'\right\rangle \left\langle k' \right| \left.\psi_\alpha\right\rangle = E_\alpha \langle k \left|\psi_\alpha\right\rangle , \tag{2.43}$$

where we have used the completeness relation.

We discretize the Schrödinger equation to get a matrix equation,

$$\sum_\gamma \varpi_\gamma k_\gamma^2 \langle k_\delta| T + V |k_\gamma\rangle \langle k_\gamma \left|\psi_\alpha\right\rangle = E_\alpha \langle k_\delta \left|\psi_\alpha\right\rangle , \tag{2.44}$$

where k_γ are the integration points and ϖ_γ are the corresponding quadrature weights.

To get a hermitian matrix we introduce $\left|\bar{k}_\delta\right\rangle = k_\delta \sqrt{\varpi_\delta} \left|k_\delta\right\rangle$. After some calculation one gets the effective interaction in the original basis $|k_\delta\rangle$,

$$\langle k_\delta| \hat{V}_{\text{eff}} |k_\gamma\rangle = \frac{\left\langle \bar{k}_\delta\right| \hat{V}_{\text{eff}} \left|\bar{k}_\gamma\right\rangle}{\sqrt{\omega_\delta \omega_\gamma} k_\delta k_\gamma}. \tag{2.45}$$

Thereafter, we transform this interaction to a harmonic oscillator basis in the laboratory frame. This interaction is used in our calculations.

2.4 Hartree-Fock

The program has a Hartree-Fock (HF) option. If this option is chosen, then it will renormalize the wavefunction with the Hartree-Fock method and use the new HF wavefunction in the perturbation theory. !Usikker paa siste setningen her.!

The purpose of the Hartree-Fock method is to replace the interaction V with an auxiliary potential U where we replace the interaction one particle feels from all the other A-1 particles by one potential for the A-1 particles.

We can ease our calculations by introducing an auxiliary potential U and rewriting the Hamiltonian

$$H = T + U + V - U = H_0 + H_1, \tag{2.46}$$

where we want to choose a U so that H_1 is small.

The Hartree-Fock method is about finding one such U. The U chosen in the Hartree-Fock method is the average interaction between one nucleon and all the other nucleons. The energy eigenvalue equation can then be rewritten as a one-particle

equation,

$$[T(x) + U_1^{HF}(x)]\phi_i(x) + \int dx' U_2^{HF}(x,x')\phi_i(x') = \varepsilon_i^{HF}\phi_i(x), \tag{2.47}$$

where

$$U_1^{HF}(x) = \sum_{j=1}^{n} \int dx' \phi_j^*(x') V_{ij}(x,x') \phi_j(x'), \tag{2.48}$$

$$U_2^{HF}(x,x') = -\sum_{j=1}^{n} \phi_j^*(x') V_{ij}(x,x') \phi_j(x), \tag{2.49}$$

and ε_i^{HF} is the Hartree-Fock energy eigenvalue for particle i.

To calculate equation 2.47 we need to know $\phi_i(x)$. In the Hartree-Fock method we choose an initial trial wavefunction $\phi_i(x)$ and initial position x of the nucleons. We then find the energy eigenvalues and eigenstates. The next step is to compare the old wavefunction $\phi_i(x)$ with the new one. If they're not sufficiently equal, then we repeat the calculations of equation 2.47 with the new $\phi_i(x)$. Then we compare that and so on until $\phi_i(x)_{old} \approx \phi_i(x)_{new}$.

For a more detailed discussion of the Hartree-Fock method, see E.K.U. Gross [11].

After these calculations, we employ many-body perturbation theory to third order.

2.5 Perturbative many–body approaches

Finally, we briefly sketch how to calculate an effective interaction in terms of the G–matrix. The first step here is to define the so–called $\hat{Q}$–box given by

$$P\hat{Q}P = PH_1P + P\left(H_1\frac{Q}{\omega - H_0}H_1 + H_1\frac{Q}{\omega - H_0}H_1\frac{Q}{\omega - H_0}H_1 + \dots\right)P, \tag{2.50}$$

where we will replace H_1 with $G - U$ (G replaces the free NN interaction V) or the Vlowk renormalized effectige interaction. The $\hat{Q}$–box[1] is made up of non–folded diagrams which are irreducible and valence linked. A diagram is said to be irreducible if between each pair of vertices there is at least one hole state or a particle state outside the model space. In a valence–linked diagram the interactions are linked (via fermion lines) to at least one valence line. Note that a valence–linked diagram can be either connected (consisting of a single piece) or disconnected. In the final expansion including folded diagrams as well, the disconnected diagrams are found to cancel out [4]. This corresponds to the cancellation of unlinked diagrams of the Goldstone expansion [4]. We illustrate these definitions by the diagrams shown in fig. 2.3, where an arrow pointing upwards (downwards) is a particle (hole) state. Particle states outside the model space are given by railed lines. Diagram (a) is irreducible, valence linked and

[1] The $\hat{Q}$–box should not be confused with the exclusion operator Q.

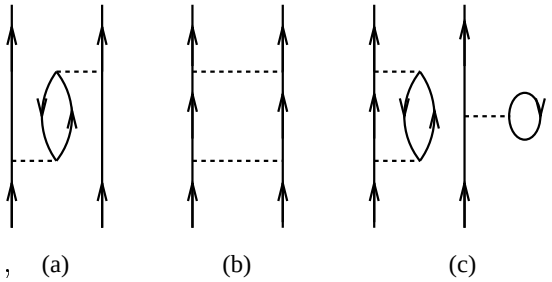

Figure 2.3: Different types of valence–linked diagrams. Diagram (a) is irreducible and connected, (b) is reducible, while (c) is irreducible and disconnected.

connected, while (b) is reducible since the intermediate particle states belong to the model space. Diagram (c) is irreducible, valence linked and disconnected.

We can then obtain an effective interaction H_{eff} in terms of the $\hat{Q}$–box, with [4]

$$H_{eff}^{(n)} = \omega + \hat{Q} + \sum_{m=1}^{\infty} \frac{1}{m!} \frac{d^m \hat{Q}}{d\omega^m} \left\{ H_{eff}^{(n-1)} - \omega \right\}^m . \tag{2.51}$$

Observe also that the effective interaction $H_{eff}^{(n)}$ is evaluated at a given model space energy ω, as is the case for the G–matrix as well. We choose this starting energy to be -20 MeV. Moreover, although $\hat{Q}$ and its derivatives contain disconnected diagrams, such diagrams cancel exactly in each order [4], thus yielding a fully connected expansion in eq. (2.51). The first iteration is then given by

$$H_{eff}^{(0)} = \omega + \hat{Q}. \tag{2.52}$$

We define the $\hat{Q}$–box to consist of all two–body diagrams[2] through third order in the G–matrix, as shown in ref. [4]. Typical examples of diagrams which are included in the $\hat{Q}$–box are shown in fig. 2.4. The summations over intermediate states is restricted to excitations of $2\hbar\Omega$ ($\hbar\Omega$ is the oscillator energy) in oscillator energy, an approximation which has been found to be appropriate if one uses a potential with a weak tensor force like the Bonn A potential. The reader should note that diagram (c) in fig. 2.4 is not included in the $\hat{Q}$–box. Three–body and other many–body effective contributions may be of importance in the study of spectra of nuclei with more than two valence nucleons. These contributions will be studied by us in future works.

Another iterative scheme which has been much favored in the literature is a method proposed by Lee and Suzuki (LS). The effective interaction we will employ in this work has been obtained using the LS method, which gives the following expression for the effective interaction

$$H_{eff}^{(n)} = \omega + \left[1 - \hat{Q}_1 - \sum_{m=2}^{n-1} \hat{Q}_m \prod_{k=n-m+1}^{n-1} \left(H_{eff}^{(k)} - \omega \right) \right]^{-1} \hat{Q}, \tag{2.53}$$

[2]With two–body we also mean one–body diagrams like diagram (a) in fig. 2.4 with a spectator valence line.

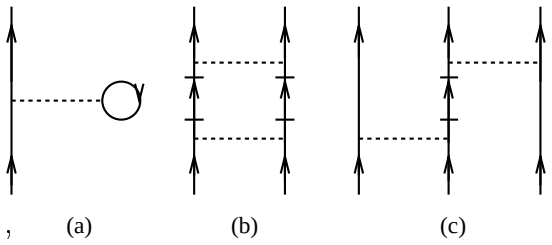

Figure 2.4: Examples of diagrams included in the $\hat{Q}$–box. Diagram (a) is a one–body diagram, whereas diagram (b) is a two–body diagram. Diagram (c) is an effective three–body diagram which is not included in our definition of the $\hat{Q}$–box.

where

$$\hat{Q}_m = \frac{1}{m!}\frac{d^m\hat{Q}}{d\omega^m}. \tag{2.54}$$

In the next chapter we will discuss the method we use to diagonalize the Hamiltonian.

Chapter 3

Shell-model calculations

We have now seen how we have reduced the full two-particle Hamiltonian in the Hilbert space to a corresponding one in our model space. We now need to solve the real, symmetric $m \times m$ matrix eigenvalue equation

$$\hat{H}_{\text{eff}} \left|\phi_k\right\rangle = E_k \left|\phi_k\right\rangle , \tag{3.1}$$

where $k = 1, \ldots, m$.

In most situations one is only interested in the states with the lowest energy, and their corresponding eigenvectors. Since the dimension of the configuration space often is quite large, we do not want to diagonalize the whole matrix. Most diagonalization methods, however, requires one to diagonalize the complete Hamiltonian.

A diagonalization method that does not require one to diagonalize the whole matrix is the Lanczos method. We discuss this method in section 2, and in section 3 we will look at how we can find the $E2$ transition strength from the diagonalized matrix. First, however, we will look at the so-called m-scheme representation of the basis states we use.

3.1 m-scheme representation

The m-scheme representation of the basis states makes numerical calculations of the eigenvalue problem relatively easy. It involves grouping the basis states after the total spin projection M, instead of grouping them after the total spin J and isospin projection T_z. I have taken much of the information here from [12].

Using the m-scheme representation will make our Hamiltonian much larger. The Hamiltonian will, however, still have rotational symmetry, and commute with J^2 and T_z. This ensures that the eigenvalues will have good J and T_z values.

We want to write the eigenstates of equation 3.1 as a linear combination of Slater

	^{14}C	^{15}C	^{15}B	^{16}C
$0p\frac{3}{2} - 0d\frac{3}{2}$	$3.2 \cdot 10^6$		$2.0 \cdot 10^6$	$7.4 \cdot 10^6$
$0p\frac{3}{2} - 0f\frac{7}{2}$	$9.7 \cdot 10^6$	$52.8 \cdot 10^6$	$76.7 \cdot 10^6$	$95.7 \cdot 10^6$

Table 3.1: Table over the dimensions of the model spaces for the different nuclei. The first coloumn lists the model spaces, while the first row lists the nuclei.

i =	1	2	3	4	5	6
m =	$-\frac{3}{2}$	$-\frac{1}{2}$	$-\frac{1}{2}$	$\frac{1}{2}$	$\frac{1}{2}$	$\frac{3}{2}$
j =	$\frac{3}{2}$	$\frac{3}{2}$	$\frac{1}{2}$	$\frac{1}{2}$	$\frac{3}{2}$	$\frac{3}{2}$

Table 3.2: Table showing the available states in the $1s\frac{1}{2}$ and $0d\frac{3}{2}$ orbitals. The number i says which state we have.

determinants, which are given by

$$|\mathrm{SD}_\nu\rangle = \prod_{jm\in\nu} a^\dagger_{jm} |c\rangle \,, \tag{3.2}$$

where $|c\rangle$ is the reference vacuum state given by equation 2.4.

We get the full basis-set by distributing the nucleons we have in every possible way over our model space, with the restriction that the total angular momentum projection M must be 0 for even nuclei and $\frac{1}{2}$ for odd nuclei. The number of states we have becomes very large for large model spaces. See table 3.1 for the dimensions of the model spaces for the different nuclei.

The Slater determinants in the m-scheme can be expressed very efficiently numerically, requiring one integer? variable for each Slater determinant. Numerically a Slater determinant can be coded as

$$|\mathrm{SD}\rangle \rightarrow (010011101000\ldots), \tag{3.3}$$

where there is one digit (bit) for every available single particle state in our Slater determinant.

The bits represent the occupancy of a state. Bit 1 indicates that a state is occupied, and bit 0 indicates that a state is unoccupied. The states are sorted first after spin projection m, then angular momentum j, then orbital spin l and finally the number of nodes $n$of the single-particle wave function.

I will illustrate this with an example. Table 3.2 shows the states we have in the $1s\frac{1}{2}$ and $0d\frac{3}{2}$ orbitals. The number i represents which state we talk about, and is unique for each state. For $i = 2$ we look at the state with $j = \frac{3}{2}$ and $m = -\frac{1}{2}$. Equation 3.4 shows a configuration with three particles in the $1s\frac{1}{2}$ and $0d\frac{3}{2}$ orbitals.

$$\left|1s_{\frac{1}{2}}, 0d^2_{\frac{3}{2}}\right\rangle = a^\dagger_{j=\frac{3}{2},m=\frac{3}{2}} a^\dagger_{j=\frac{3}{2},m=-\frac{1}{2}} a^\dagger_{j=\frac{1}{2},m=-\frac{1}{2}} |c\rangle$$
$$= a^\dagger_2 a^\dagger_3 a^\dagger_6 |c\rangle \tag{3.4}$$

The calculations used when we let the Hamiltonian operate on a state of this type are simple. Let us give an example of this. We write our Hamiltonian as

$$\hat{H}_{\text{eff}} = \sum_{i=1}^{d} \epsilon_i a^\dagger_i a_i + \frac{1}{4} \sum_{ijkl}^{d} \langle ij| \hat{V}_{\text{eff}} |kl\rangle \, a^\dagger_i a^\dagger_j a_l a_k. \tag{3.5}$$

where d is the dimension of the Hamiltonian matrix.
!Tror at det er d istedenfor A. d er det samme som m i forklaringen til ligning 3.1.!

We look at the configuration $i = 1$, $j = 4$, $k = 6$, $l = 2$. We then get

$$a^\dagger_1 a^\dagger_4 a_2 a_6 (011001) = -a^\dagger_1 a^\dagger_4 (001000)$$
$$= -(101100). \tag{3.6}$$

This illustrates the simplicity of calculations in the m-scheme representation.

We have seen that the m-scheme representation will make computations with the Slater determinants relatively easy, the drawback being that our Hamiltonian matrix gets much larger. We will now go on to discuss how we will actually diagonalize our Hamiltonian with the Lanczos method.

3.2 Lanczos' method

We will use the Lanczos method to diagonalize the effective two-particle Hamiltonian in the m-scheme basis. One of the main advantages of the Lanczos method is that we do not have to diagonalize the whole matrix. I will below outline this method. For more details see [13], and [14]

1. One chooses an initial Lanczos' vector $|lanc_0\rangle$ as a 0th order approximation to the eigenvalue equation $H|\psi_k\rangle = E_k|\psi_k\rangle$, with $k = 1, \ldots, K$. K is the size of of the H_{eff} matrix. The initial Lanczos' vector should not have good angular momentum, as the iteration would then terminate too early.

2. A new vector is generated by letting the Hamiltonian work on the Lanczos vector: $|new_{p+1} >= H|lanc_p >$, where p goes from 0 to $K-1$. The diagonal matrix elements of H can now be found by

$$\langle lanc_p| H |lanc_p\rangle = \langle lanc_p| \, new_{p+1}\rangle \, . \tag{3.7}$$

3. We orthogonalize the Lanczos vectors by

$$\left|new'_{p+1}\right\rangle = |new_{p+1}\rangle - |lanc_p\rangle \cdot \langle lanc_p|\ new_{p+1}\rangle - \sum_{q=0}^{p-1} |lanc_q\rangle \cdot \langle lanc_q|\ new_{p+1}\rangle\,, \tag{3.8}$$

and normalize it,

$$|lanc_{p+1}\rangle = \frac{1}{\sqrt{\left\langle new'_{p+1}\right|\ new'_{p+1}\rangle}} \left|new'_{p+1}\right\rangle. \tag{3.9}$$

This produces a new Lanczos' vector.

4. The off-diagonal matrix elements of H can now be calculated by

$$\langle lanc_{p+1}|\, H\, |lanc_p\rangle = \left\langle new'_{p+1}\right|\ new'_{p+1}\rangle\,. \tag{3.10}$$

The other matrix elements are zero.

5. After n iterations we will have a tri-diagonal matrix of the form

$$H_n = \begin{Bmatrix} H_{0,0} & H_{0,1} & 0 & \cdots & 0 \\ H_{0,1} & H_{1,1} & H_{1,2} & \cdots & 0 \\ 0 & H_{2,1} & H_{2,2} & \cdots & 0 \\ \vdots & \vdots & \vdots & \vdots & H_{p-1,p} \\ 0 & 0 & 0 & H_{p,p-1} & H_{p,p} \end{Bmatrix}. \tag{3.11}$$

6. This process is repeated until we have a convergence, that is $H_n \approx H_{n-1}$.

A problem with the Lanczos method is that it uses a lot of data storage. When m gets large, the size of each Lanczos' vector also increases. The storage capacity needed gets very large when the number of Lanczos' vectors increases beyond 100. However, to get a good convergence, we usually need a big number of Lanczos' vectors, as the Lanczos method has a slow rate of convergence.

In our program we stop when we have reached a suitable convergence criteria for the angular momenta, or when we reach the maximum number of iterations specified at the start of the calculation. If we reach the iteration limit before we have a convergence, we then need to look at the angular momentum J from the program output. If the state we look at has a converged value for the angular momentum, then that state has converged. In the energy spectrum figures in chapter 4 I have only included those energy states that have a converged value for the angular momentum.

The Lanzos method gives us, in addition to the energy for the excited states, also their eigenvectors. These eigenvectors can be used to find the electromagnetic transitions between the states.

3.3 Electromagnetic transitions

We will here show how to calculate the electromagnetic transitions. We will concentrate on the E2 transition for even nuclei.

The electromagnetic transitions can be divided into electric and magnetic transitions, and are defined by the spherical harmonics Y_μ^L. For $L = 2$ both the E2 and the M2 transitions are possible, but they have differing parity. The electric transitions are much more probable than the magnetic transitions for equal values of L.

The theory for electromagnetic transitions is based on Maxwell's equations for a propagating electromagnetic field.

The interaction Hamiltonian is given as (see Brussaard and Glaudemans [15] for details)

$$H_{e.m.} = \frac{1}{c}\int \mathbf{j}(\mathbf{r},t)\mathbf{A}(\mathbf{r},t)d\mathbf{r} + \int \rho(\mathbf{r},t)\phi(\mathbf{r},t)d\mathbf{r}, \tag{3.12}$$

where $\mathbf{j}(\mathbf{r},t)$ represents the current density, and $\rho(\mathbf{r},t)$ represents the charge density, of the nucleus. $\mathbf{A}(\mathbf{r},t)$ is a vector potential and $\phi(\mathbf{r},t)$ is a scalar potential.

The transverse gauge condition is

$$\nabla\mathbf{A}(\mathbf{r},t) = 0. \tag{3.13}$$

The transverse gauge condition reflects the fact that the photon only has two independent polarization states.

The transition rate T, that is the transition probability per time, for a transition between an initial state i and final state f, is given as [15],

$$T(L) = \frac{8\pi(L+1)}{L[(2L+1)!!]^2}\frac{k^{2L+1}}{\hbar}B(L), \tag{3.14}$$

where B(L) is the "reduced transition probability" defined as

$$B(L) = \frac{|\langle J_f|\,|\hat{O}(L)|\,|J_i\rangle|^2}{2J_i+1}. \tag{3.15}$$

Here the Wigner-Eckarts theorem has been used to define the reduced matrix element

$$\langle njm|\,T_\mu^\lambda\,|n'j'm'\rangle = \langle nj|\,|T^\lambda|\,|n'j'\rangle\,C^{jm}_{\lambda\mu j'm'}, \tag{3.16}$$

where $C^{jm}_{\lambda\mu j'm'}$ is a Clebsch-Gordan coefficient.

The initial and final states for systems where one photon is emitted, as is the case in our calculations, can be written as

$$|I\rangle = |J_iM_i\rangle\,|F\rangle = |J_fM_f, 1_{k,\alpha}\rangle\,, \tag{3.17}$$

where $1_{k,\alpha}$ is a one-photon state.

The electromagnetic transition depends on the reduced matrix elements,

$$\langle F|\,\hat{O}\,|I\rangle \tag{3.18}$$

where $\hat{O}$ is the sum of the electric and magnetic multipole operators

$$\hat{O} = \sum_{L,\mu} \left(\hat{O}(EL)_\mu + \hat{O}(ML)_\mu \right). \tag{3.19}$$

The electric transition operator [15] is given by

$$O(EL)_\mu = \sum_{k=1}^{A} e(k) r^L(k) Y_\mu^L(\mathbf{r}), \tag{3.20}$$

where Y_μ^L are the spherical harmonics and $e(k)$ is the electric charge for nucleon k. In our calculations the electric charge will be replaced by the effective electric charge, as the neutron, while neutral as a whole, feels an effective charge from the neutrons and protons in the closed core. The same is true for the proton. The value of the effective charges are adjusted to fit the experimental data.

The reduced transition probability for E2 transitions can be written as

$$B(E2, L) = \frac{1}{2J_i + 1} |\,\langle J_f|\,|\sum_k e_k r_k^2 Y^2(\theta_i \phi_i)|\,|J_i\rangle\,|^2. \tag{3.21}$$

The program finds the reduced matrix elements of 3.21 by using the eigenvectors that we found with the Lanczos method. It then uses these reduced matrix elements to find the transition probability for a given L.

With this we have now briefly discussed the physics behind the program. We will in the next chapter go on to look at the results from our computations.

Chapter 4

Results

We will here look at the energy spectra for ^{14}C, ^{15}C, ^{15}B and ^{16}C, and selected excitation strengths for $B(E2)$ of ^{14}C and ^{16}C. We will begin by discussing the energy spectra for each nucleus, starting with ^{14}C and ending with ^{16}C. We will then discuss the excitation strengths we got for ^{14}C and ^{16}C.

As mentioned earlier, I used two sets of single particle (sp) energies: Those that the program calculated, and those given by E. K. Warburton and B. A. Brown in Ref. [3] for ^{16}O. During the calculations it became apparent that the sp energies from Brown's article gave excitation energies, for all four nuclei, that were in much better agreement with the experimental values. Also, when I used the sp energies that the program calculated, the states had a slow rate of convergence in the Lanczos method. See figures 4.1 and 4.3 for a comparison between the program's sp energies and Brown's sp energies.

Figures 4.1 and 4.2 each show four different calculations done in the same model space. The calculations with a Hartree-Fock basis gave worse excitation energies than the calculations without Hartree-Fock. We see this behaviour for the other nuclei too. The Hartree-Fock single-particle energies result in a single-particle gap which is much larger than the experimental values. This results in large enery denominators when we do many-body perturbation theory and thereby an effective interaction which is smaller on average than the one obtained using hamronic oscillator energies. The final result is an excitation spectrum which is more compressed. Because of this I will not include calculations with Hartree-Fock in our discussions of the nuclei.

In figures 4.1 and 4.2 we see that the G-matrix and Vlowk methods give almost identical energy spectra. This is also the case for the other calculations in the $0p\frac{3}{2}-0d\frac{3}{2}$ model space. I cannot tell from the figures which is best, but the Vlowk method depends strongly on the chosen cutoff in momentum space. A larger cutoff produces smaller matrix elements and thereby a more compressed spectrum. On the other hand, a smaller cutoff than that chosen here, leads to larger effective matrix elements. Unless the two-body interactionis accompanied by a three-body interaction or higher-body interaction computed with the same cutoff value, many-body correlations will be large when doing shell-model calculations. I will therefore use the G-matrix method in our discussions of the nuclei.

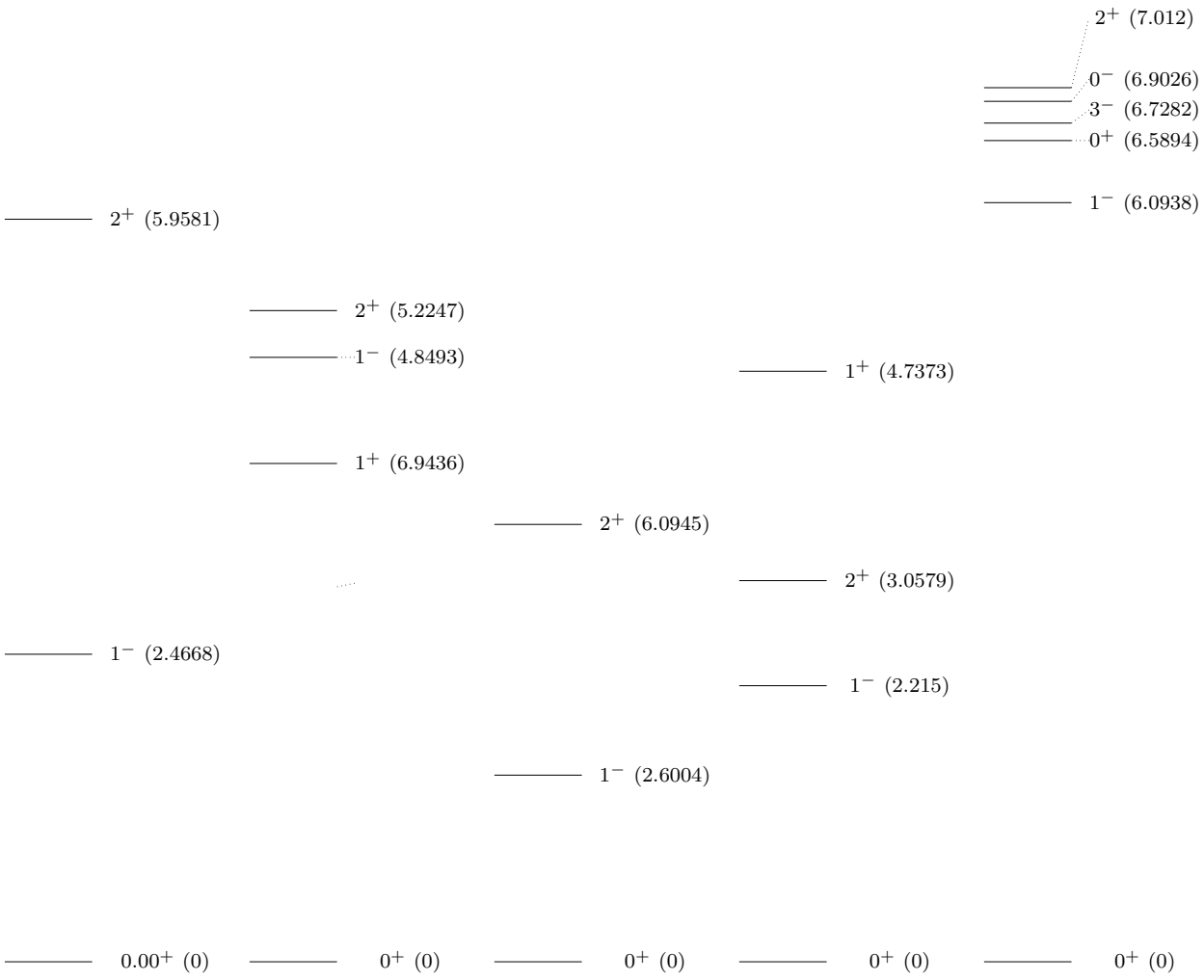

Figure 4.1: Energy spectra for ^{14}C, in the 0p3-0d3 model space, using 3. order perturbation theory. The spectra have been found using the orbital-energies from the program. 'HF' here means Hartree-Fock. 'G-matrix' and 'Vlowk' are different renormalization methods, see chapter 2 for details. The energies are given in MeV.

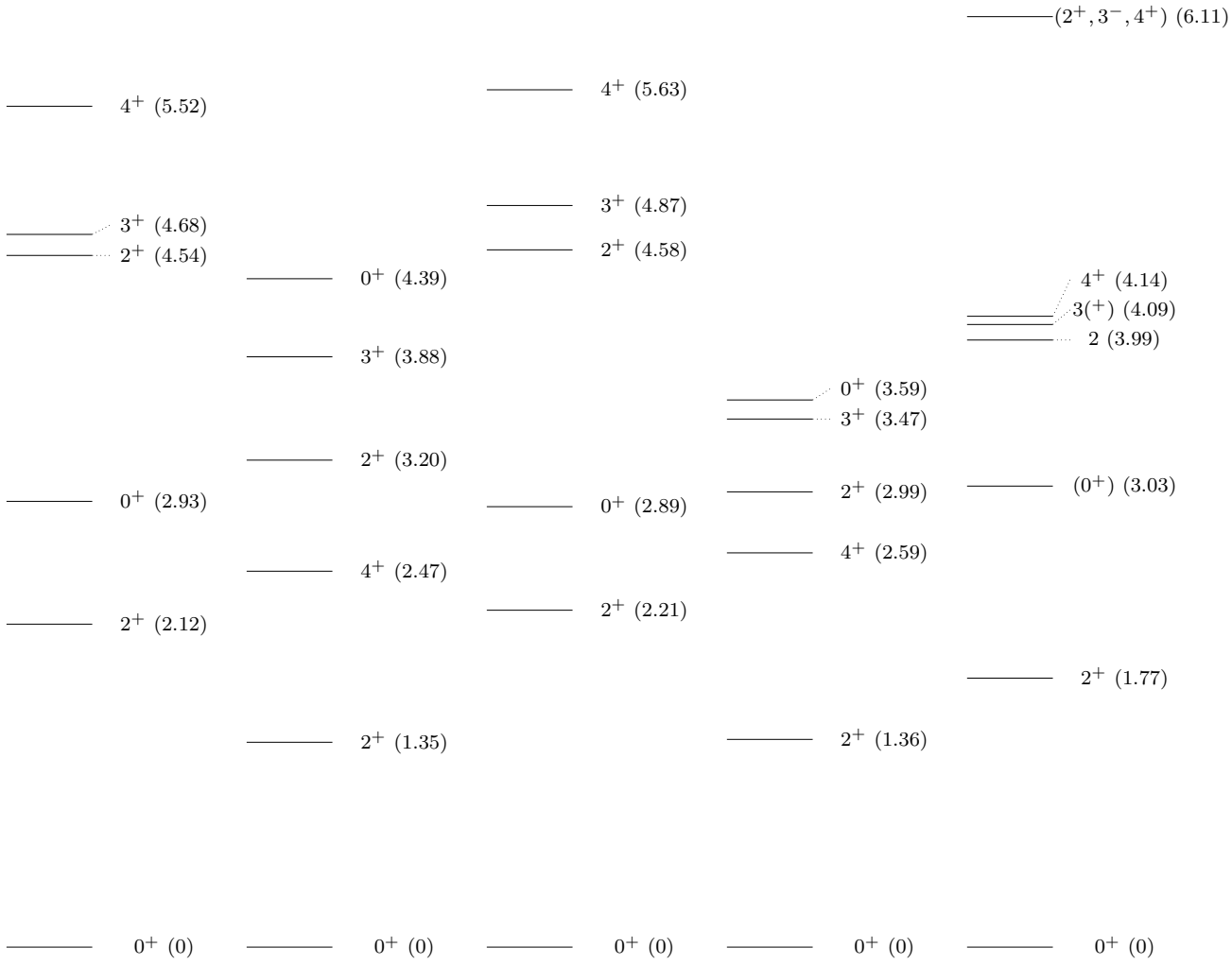

Figure 4.2: Energy spectra for 16C, in the 0p3-1s1 model space. The spectra have been found using the orbital-energies for ^{16}O given by B.A. Brown and E.K. Warburton [1]. 'HF' here means Hartree-Fock. 'G-matrix' and 'Vlowk' are different renormalization methods, see chapter 2 for details. The energies are given in MeV.

The energy spectra for the final results are given in figures 4.3, 4.8, 4.11 and 4.16. Unless otherwise notified in the figure labels, each figure has been calculated using: the orbital-energies for ^{16}O given by B.A. Brown and E.K. Warburton [3], the G-matrix method without Hartree-Fock, full $0p\frac{3}{2} - 0d\frac{3}{2}$ model space, a $0p\frac{3}{2} - 0f\frac{7}{2}$ model space reduced by only allowing 4 neutrons and 4 protons in the $0d\frac{5}{2}$orbital, and 2 neutrons and 2 protons in each of the $0d\frac{3}{2}$ and $0f\frac{7}{2}$ orbitals. For ^{15}C and ^{16}C the $0p\frac{3}{2} - 0f\frac{7}{2}$ model space has been reduced further by allowing 0 protons to ecxite to the $0f\frac{7}{2}$ orbital.

The energy spectra on the right side of the figures show the experimental excitation energies. For ^{16}C and especially ^{15}B only the lowest energy states have been found experimentally. For ^{14}C (see figure 4.3) I have included only those excitation states with energies below 12 MeV. This is because above 12 MeV there are no states with angular momenta 1^-, 0^+ and 2^+ in the experimental data, and no states with angular momentum 3^- above 16 MeV [16].

The first number in each energy spectrum is the angular momentum of that excited state, with the parity also given. The next number, given in parenthesis, is the energy difference (in MeV) between the ground state and that excited state. The excited states are characterized by the angular momentum, parity and energy. The first line in each energy spectrum is the ground state. The experimental angular momenta and parity sometimes have parenthesis around them. This means that there is some uncertainty regarding these values. GE means greater than or equal to.

Figures 4.4-4.7, 4.9-4.10, 4.17-4.20 and 4.12-4.15. show the sp orbital occupancy for ^{14}C, ^{15}C, ^{16}C and ^{15}B. I have here also only looked at results calculated with the G-matrix method, without a Hartree-Fock single-particle basis. The figures for the ground state show how many protons and neutrons are in each orbital as a bar diagram. The figures for the excited states show the occupation difference between that excited state and the ground state. I have only included figures for the ground state and the first excited state, as it is the first excited 2^+ state that we are interested in.

Tables 4.1-?? show the orbital occupancy for the ground state and excited states and the orbital occupancy difference form the ground state for the first three excites states of each nucleus. Though we are mainly interested in the first excited 2^+ state, I do discuss the other excited states. While the bar diagrams give us a better overall picture of the orbital occupancies, the added tables list the numerical values as well.

We notice in the orbital occupancy figures that the occupancy of the ground state differs from our model's occupancy (see for example figure 1.3). The simple model presumes one single Slater determinant. Our final wavefunction, on the other hand, includes the effect correlations as well, mixing many Slater determinants. This means in turn that single-particle occupancy can be higly fragmented.

The $0p\frac{3}{2} - 1s\frac{1}{2}$ model space quickly proved to be too small (see figure 4.2), as the results did not correspond well with the experimental data. We therefore had to include the $0d\frac{3}{2}$ orbital in our model space. The results from the calculations in the $0p\frac{3}{2} - 0d\frac{3}{2}$ model space are given, with the results from the calculations in the $0p\frac{3}{2} - 0f\frac{7}{2}$ model space, in figures 4.3, 4.11 and 4.16. We see from the energy spectra that the excitation energies had not yet converged in the $0p\frac{3}{2} - 01s\frac{1}{2}$ model space. The results

are, however, still rather different from the experimental values, and we need to include the next orbital (the $0f\frac{7}{2}$ orbital) to see if the excitation energies have converged as functions of the model spaces.

To test if the excitation energies had stabilized, I ran the program in the $0p\frac{3}{2} - 0f\frac{7}{2}$ model space. Because this model space is over 50 times larger than the $0p\frac{3}{2} - 0d\frac{3}{2}$ model space, using the full model space would be too large for the computers I used. Therefore I needed to reduce the model space. If one looks at figures 4.12 and 4.13 of the occupancy of single particle orbitals for the ground state and the first excited state of ^{15}B, one sees that the $0d\frac{3}{2}$ orbital has an average of under 0.3 particles in it, and the $0d\frac{5}{2}$ orbital has under 1.8 particles. The $0f\frac{7}{2}$ orbital should have even less particles in it than the $0d\frac{3}{2}$ orbital. I should therefore get a good result if I make an approximation with only 4 neutrons and protons allowed in the $0d\frac{5}{2}$ orbital and 2 neutrons and protons in the $0d\frac{3}{2}$ and $0f\frac{7}{2}$ orbitals. To test this, I ran a simulation with reduced $0p\frac{3}{2} - 0d\frac{3}{2}$ model space, 4 neutrons and protons in the $0d\frac{5}{2}$ orbital and 2 neutrons and protons in the $0d\frac{3}{2}$ orbital. For ^{15}C and ^{16}C I reduced the $0p\frac{3}{2} - 0f\frac{7}{2}$ model space further by allowing 0 protons to excite to the $0f\frac{7}{2}$ orbital. The result is shown in figure 4.11. We see that the energy spectrum for the reduced model space is very similar to the energy spectrum for the full model space. The reduced $0p\frac{3}{2} - 0f\frac{7}{2}$ model space mentioned above should therefore be a good approximation. I will also only calculate the first four states for odd and even parity, as this will also reduce the computing time.

I expected that the $0f\frac{7}{2}$ orbital would have small impact on the interaction, as there would be a very low number of particles in it, however, it proved to have a significant impact on the energy spectra. See figures 4.3, 4.8, 4.11 and 4.16. The figures shows that the excitation energies had not converged yet for the $0p\frac{3}{2} - 0d\frac{3}{2}$ model space. The $1p\frac{3}{2}$ orbital should be included in our model space to see if we have convergence. However the model space will then be too big to calculate with the present version of the shell-model code and within the time limts of a Master of Science thesis.

We shall now look closer at our results, starting with ^{14}C.

4.1 ^{14}C

There have been done many calculations on ^{14}C. Most have used a model space based solely on the $0p$ shell, looking at a two-proton hole situation. With careful adjustments of the interaction, one can obtain a good correspondence with the experimental states with positive parity. (The excitations cannot have negative parity as they only excite within the $0p$ shell and thus do not change l-value for a two-hole state.) Calculations mixing the $0p$ and $1s0d$ shells have been difficult to do. Our results will hopefully show if one needs to include the $1s0d$ shell, and possibly the $0f1p$ shell to get states corresponding to the experimental states, or if it is enough to only calculate in the $0p$ shell, without adjusting the interaction to fit the experimental values.

We see in figure 4.3 that we predict several of the experimental states, most notably the first 2^+ state. The energy correspondence of these states to the experimental states is not good for the $0p\frac{3}{2} - 0d\frac{3}{2}$ model space. For the $0p\frac{3}{2} - 0f\frac{7}{2}$ model space it gets

considerably better, though we have too few states to say anything conclusive about this model space.

Another thing to note is that the orbital occupancy in the $0p\frac{3}{2} - 0f\frac{7}{2}$ model space is almost identical to the orbital occupancy in the $0p\frac{3}{2} - 0d\frac{3}{2}$ model space, see figures 4.4-4.7)) and tables 4.1-4.4). The orbital occupancies also shows that ^{14}C is ruled mostly by proton excitations, except for the second 2^+ state.

4.1.1 $0p\frac{3}{2} - 0d\frac{3}{2}$ model space

Figure 4.3 shows the energy spectra for ^{14}C. We will look at the energy spectrum in the $0p\frac{3}{2} - 0d\frac{3}{2}$ model space here. Two things come to our notice. One being that there are some experimental states that we have not predicted, such as the first 0^+ and 4^+ states. The other is that our states have too high energy, especially for the high-lying states. It is difficult to say what this high energy difference comes from, as there are several things that might cause this. The nucleus ^{14}C has a high amount of resonance dependent states. We cannot hope to predict these states, as our effective interaction is derived using a harmonic oscillator basis. We also do not take into account Center of Mass Corrections. The amount of spurious center of mass contamination has not been evaluated in this thesis and needs to be done prior to an eventual publication of these results.

In our ground state (see figure 4.4) we have roughly 3.5 protons in the $0p\frac{3}{2}$ orbital and 0.5 protons in the $0d\frac{5}{2}$ orbital. For neutrons we have roughly 3.5 neutrons in the $0p\frac{3}{2}$ orbital, 2 neutrons in the $0p\frac{1}{2}$ orbital and 0.5 protons in the $0d\frac{5}{2}$ orbital. We see that this is very close to our single particle picture of ^{14}C's ground state 1.1.

The first 2^+ state corresponds to the experimental first 2^+ state, though we do not get a good energy correspondence, with the energy being about 0.5 MeV above the experimental value. The excitation is mainly a one-neutron excitation from the $0p\frac{3}{2}$ orbital to the $0p\frac{1}{2}$ orbital. (See figure 4.5.)

For the 1^+ state we see that we have two experimental states. We have one state where they believe the angular momentum to be greater than or equal to 1 (they do not know its parity). Its energy is about 0.7 MeV (6.6%) lower than our predicted state. There is another state with angular momentum 1^+ that lies roughly 0.2 MeV (1.5%) higher than our predicted state. This is quite near our state.

We do not have the first 0^+ state nor the 4^+ and higher-lying states. Our predicted second 2^+ state, 0^+ state and third 2^+ state seems to correspond with the experimental second 2^+ state, second 0^+ state and third 2^+ state, though our states lie roughly 6-7 MeV (over 50%) above the experimental states. Our three states are close to each other though, with an equal energy gap between them, which the experimental states also have. Because of this I believe our second 2^+, first 0^+ and third 2^+ states to correspond to the experimental second 2^+, second 0^+ and third 2^+ states.

4.1.2 $0p\frac{3}{2} - 0f\frac{7}{2}$ model space

We will now look at the energy spectrum in the $0p\frac{3}{2} - 0f\frac{7}{2}$ model space shown in figure 4.3.

We see that the first 2^+ state is now very close to the experimental state, with an excitation energy difference of roughly 0.03 (0.14%).

The 1^+ state is almost unchanged, which means that we most likely have a convergence for this state. Again I cannot say for sure which experimental 1^+ state it corresponds to, though the experimental 1^+ state at 11.306 MeV seems likely, as it is much closer to our 1^+ state.

The second 2^+ state has had its energy lowered by roughly 3.6 MeV, and is now considerably closer to both the second and third experimental 2^+ states. From our discussion about the $0p\frac{3}{2} - 0d\frac{3}{2}$ model space this state most likely corresponds to the second experimental 2^+ state. We see that the orbital occupation for this state is actually not dominated by proton excitations but have an almost equal number of proton and neutron excitations, going mostly from the $0p\frac{3}{2}$ orbital to the $0d\frac{5}{2}$ orbital. This state is the only one of the five excited states with positive parity I have predicted that is not ruled by proton excitations

In conclusion I want to say that the $0p\frac{3}{2} - 0d\frac{3}{2}$ model space is enough to predict several of the experimental states, but we do not get a good energy correlation. The $0p\frac{3}{2} - 07\frac{7}{2}$ model space seems to considerably improve the reproduction of the experimental results, but we have too few states to be able to draw a conclusion about how much of an improvement the $0p\frac{3}{2} - 07\frac{7}{2}$ model space is.

It should be enough with the $0p$ shell to predict most of the states. To get the second 2^+ state, however, one needs to include the $1s0d$ shell in one's calculations.

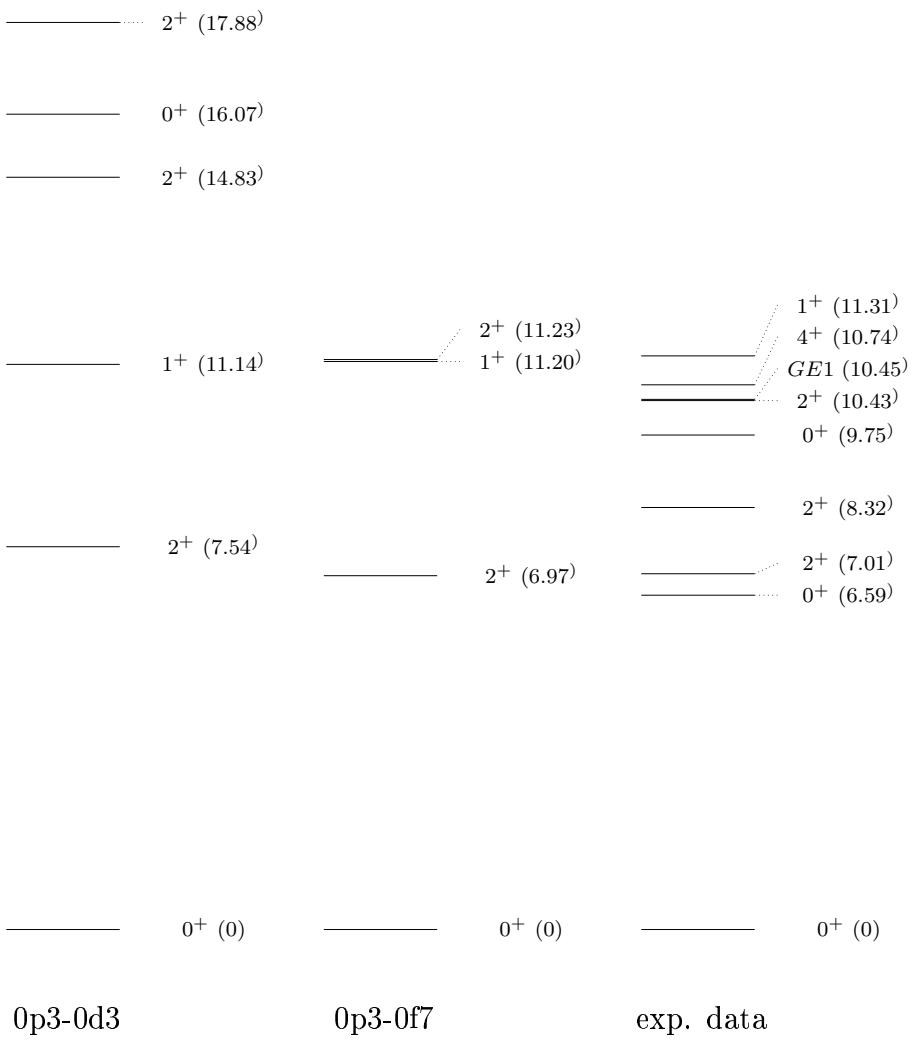

Figure 4.3: Energy spectra for 14C, in the full 0p3-0d3 and reduced 0p3-0f7 model spaces. By reduced 0p3-0f7 model space we mean that we have reduced our 0p3-0f7 model space so that we have a maximum of 4 particles in the 0d5 orbital, a maximum of 2 particles in the 0d3 orbital and a maximum of 2 particles in the 0f7 orbital. The energies are given in MeV.

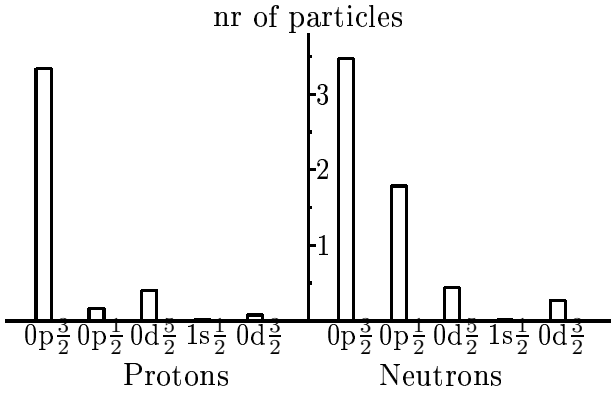

Figure 4.4: Orbital occupation for the groundstate state of ^{14}C with orbital momentum $J = 0^+$, in the 0p3-0d3 model space.

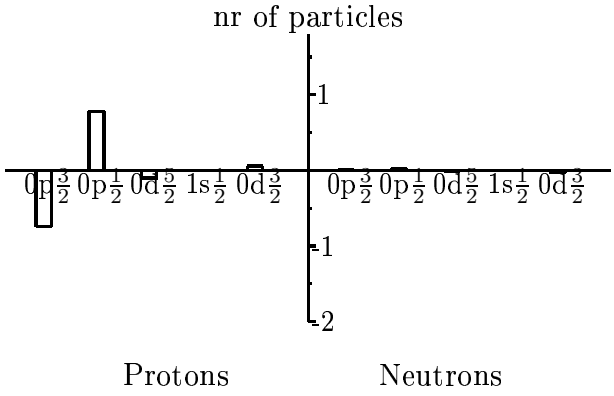

Figure 4.5: Orbital occupation difference from the ground state for the first 2^+ state of ^{14}C, in the 0p3-0d3 model space.

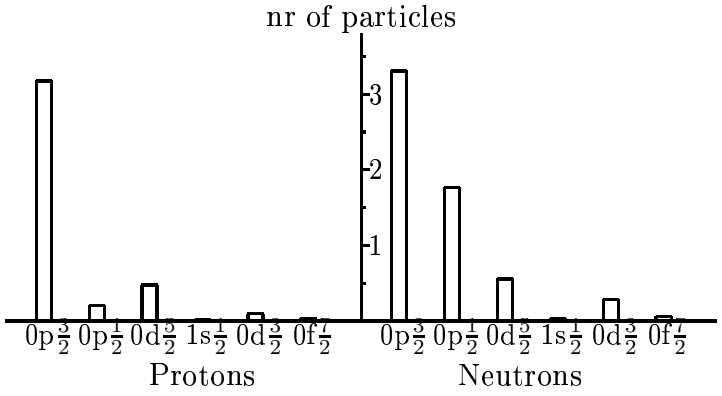

Figure 4.6: Orbital occupation for the ground state of ^{14}C with orbital momentum $J = 0^+$, in the 0p3-0f7 model space.

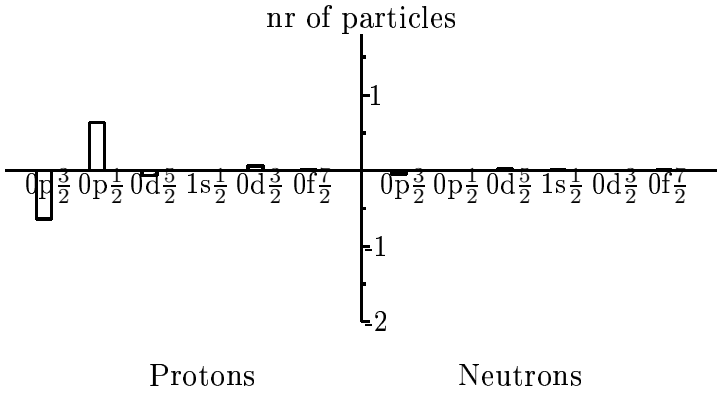

Figure 4.7: Orbital occupation difference from the ground state for the first2^+ state in ^{14}C, in the 0p3-0f7 model space.

Protons	$0p\frac{3}{2}$	$0p\frac{1}{2}$	$0d\frac{5}{2}$	$1s\frac{1}{2}$	$0d\frac{3}{2}$
Ground state $J = 0^+$	3.34	0.17	0.40	0.02	0.08
First 2^+ state	-0.74	+0.79	-0.10	0.00	+0.05
First 1^+ state	-0.71	+0.75	-0.09	0.00	+0.05
Second 2^+ state	-0.48	+0.03	+0.31	+0.07	+0.07

Table 4.1: Proton orbital occupancy for ^{14}C in the $0p\frac{3}{2} - 0d\frac{3}{2}$ model space. The horizontal line gives the orbitals, and the vertical line gives the excited states. For the excited state the diagram shows the orbital occupancy difference from the ground state.

Neutrons	$0p\frac{3}{2}$	$0p\frac{1}{2}$	$0d\frac{5}{2}$	$1s\frac{1}{2}$	$0d\frac{3}{2}$
Ground state $J = 0^+$	3.47	1.79	0.45	0.02	0.27
First 2^+ state	+0.02	+0.01	-0.01	+0.01	-0.03
First 1^+ state	+0.03	+0.02	-0.02	0.00	-0.03
Second 2^+ state	-0.56	-0.26	+0.46	+0.07	+0.29

Table 4.2: Neutron orbital occupancy for ^{14}C in the $0p\frac{3}{2} - 0d\frac{3}{2}$ model space. The horizontal line gives the orbitals, and the vertical line gives the excited states. For the excited state the diagram shows the orbital occupancy difference from the ground state.

Protons	$0p\frac{3}{2}$	$0p\frac{1}{2}$	$0d\frac{5}{2}$	$1s\frac{1}{2}$	$0d\frac{3}{2}$	$0f\frac{7}{2}$
Ground state $J = 0^+$	3.18	0.21	0.47	0.02	0.09	0.03
First 2^+ state	-0.64	+0.64	-0.06	0.00	+0.06	+0.01
First 1^+ state	-0.64	+0.69	-0.10	0.00	+0.05	-0.01
Second 2^+ state	-0.51	+0.12	+0.23	+0.05	+0.06	+0.05

Table 4.3: Proton orbital occupancy for ^{14}C in the $0p\frac{3}{2} - 0f\frac{7}{2}$ model space. The horizontal line gives the orbitals, and the vertical line gives the excited states. For the excited state the diagram shows the orbital occupancy difference from the ground state.

Neutrons	$0p\frac{3}{2}$	$0p\frac{1}{2}$	$0d\frac{5}{2}$	$1s\frac{1}{2}$	$0d\frac{3}{2}$	$0f\frac{7}{2}$
Ground state $J = 0^+$	3.31	1.77	0.55	0.03	0.28	0.06
First 2^+ state	-0.04	-0.01	+0.03	+0.01	0.00	+0.01
First 1^+ state	+0.06	+0.01	-0.03	0.00	-0.02	-0.02
Second 2^+ state	-0.51	-0.17	+0.38	+0.03	+0.18	+0.08

Table 4.4: Neutron orbital occupancy for ^{14}C in the $0p\frac{3}{2} - 0f\frac{7}{2}$ model space. The horizontal line gives the orbitals, and the vertical line gives the excited states. For the excited state the diagram shows the orbital occupancy difference from the ground state.

4.2 ^{15}C

For ^{15}C we see from the orbital occupancy figures 4.9 and 4.10, and the orbital occupancy tables **??** and 4.6 that this nucleus is governed mostly by the excitation of one neutron from the $1s\frac{1}{2}$ orbital to the $0d\frac{5}{2}$ orbital. This means that the physics we have for ^{15}C is different from that of ^{14}C. It is interesting that the same Hamiltonian can predict these different behaviors. The neutron dominance is also in agreement with our expectations. Due to time limits we have only done calculations in the $0p\frac{3}{2} - 0f\frac{7}{2}$ model space for ^{15}C.

4.2.1 $0p\frac{3}{2} - 0f\frac{7}{2}$ model space

Figure 4.8 shows the energy spectra for ^{15}C in the $0p\frac{3}{2} - 0f\frac{7}{2}$ model space. From the figure we see that our energy spectrum corresponds somewhat with the experimental data. We have a corresponding experimental state for most of our excited states, the exception being our $\frac{7}{2}^-$ state.

For the ground state (see figure 4.9) we see that the proton configuration is almost identical to that for ^{14}C and ^{16}C. For the neutrons we have almost one neutron more in the $1s\frac{1}{2}$ orbital compared to the ground state of ^{14}C. ^{16}C has nearly 1 neutron more in the $0d\frac{5}{2}$ orbital, and a slight amount more in the $0f\frac{7}{2}$ orbital. This shows that a Slater determinant based on an occupancy of the same orbitals as ^{14}C plus one neutron is a good approximation, as when we add (subtract) a nucleon to (from) the nucleus, most of it will enter (leave) one orbital, instead of being widely scattered among several orbitals.

One point of interest here is that the neutron added to ^{14}C goes to the $1s\frac{1}{2}$ orbital instead of going to the $0d\frac{5}{2}$ orbital, which means that the $0d\frac{5}{2}$ orbital lies above the $1s\frac{1}{2}$ orbital in energy. This reflects experimental findings for ^{15}C, where the first experimental state has angular momentum $\frac{1}{2}^+$, meaning that the valence neutron outside the $0p$ shell lies in the $1s\frac{1}{2}$ orbital. Also, the experimental first excited state has angular momentum $\frac{5}{2}^+$. The ordering of both the experimental and our $0d\frac{5}{2}$ and $1s\frac{1}{2}$ orbitals are the opposite of the ordering of our sp orbitals. It is good to see that our program manages to get the same angular momenta as the experimental ground state, even though our sp orbital does not have the same order.

For the excited states I have mostly neutron excitations from the $1s\frac{1}{2}$ orbital to the $0d\frac{5}{2}$ orbital (see figure 4.10). This is in accordance with our observations of ^{16}C, where the added neutron goes to the $0d\frac{5}{2}$ orbital.

For the first $\frac{5}{2}^+$ state, we have almost a 1p1h neutron excitation from the $1s\frac{1}{2}$ to the $0d\frac{5}{2}$ orbital. This excitation has, according to theory, an angular momentum of either $\frac{5}{2} - \frac{1}{2} = 2$ or $\frac{5}{2} + \frac{1}{2} = 3$, and a parity shift of $\pi = (-1)^2 = 1$. This is in accordance with our predicted angular momentum and parity of $\frac{5}{2}^+$. This excited state corresponds with the first experimental $\frac{5}{2}^+$ state, and has and energy difference of 0.225 MeV, or 30.3% less than the experimental value.

Our $\frac{7}{2}^-$ state might be the experimental $\frac{7}{2}$ state with energy 6.449 MeV, but the energy difference is quite large, being approximately 3.76 MeV. We also see that it has a large excitation to the $0f\frac{7}{2}$ orbital, having almost a 1p1h neutron excitation from the $1s\frac{1}{2}$ orbital that spreads evenly among the $0d\frac{5}{2}$ and $0f\frac{7}{2}$ orbitals. Something that might explain part of this value is that, since this state has an excitation of half a neutron to the $0f\frac{7}{2}$ orbital, increasing the number of possible neutron excitations to 3 or more could increase the number of excited neutrons by a significant amount. However, I do not think that this will be enough to bring the $\frac{7}{2}^-$ state up to the energy level of the experimental $\frac{7}{2}$ state at 6.417 MeV. It may also be that the energy of this state is correct, and it has simply not been measured yet.

Another way to study the properties of these excited states is to perform a seniority analysis and study the quasi-particle content of these excited states.

The $\frac{3}{2}^-$ and $\frac{5}{2}^-$ states appear in the opposite order of the corresponding experimental states, and is not too far from the experimental states in energy. For the $\frac{3}{2}^-$ state we have about 0.5 neutrons that excite from the $0p\frac{3}{2}$ and $1s\frac{1}{2}$ orbitals to the $0d\frac{5}{2}$ orbital.

Our $\frac{1}{2}^-$ state also appears in an unexpected place. When we look at the ordering of the states, it seems to correspond better with the second experimental $\frac{1}{2}^-$ state. However, the ordering of the states here does not seem to be good, so it might also be the first experimental $\frac{1}{2}^-$ state.

Our second $\frac{5}{2}^+$ state corresponds to the $\frac{5}{2}$ experimental state at 6.358 MeV, having an energy difference of 7.42% of the experimental value.

Our$\frac{7}{2}^+$ state most likely corresponds to the first experimental $\frac{7}{2}^+$ state, having an energy difference of 2.47% of the experimental value.

Our calculations of ^{15}C does not correspond to the experimental results to a satisfying degree. It gives an acceptable picture of the experimental states, but the energy of our theoretical states is in general too low, and we have a different ordering of the states. This can be caused by the lack of Center of Mass Corrections, too small model space and too much limitations on the number of particles allowed to excite up to the higher-lying states (as seems to be the case with the $\frac{7}{2}^-$ state). Eventual three-body contribuitions, either effective ones of from three-nucleon interactions could also influence the description of some of these states.

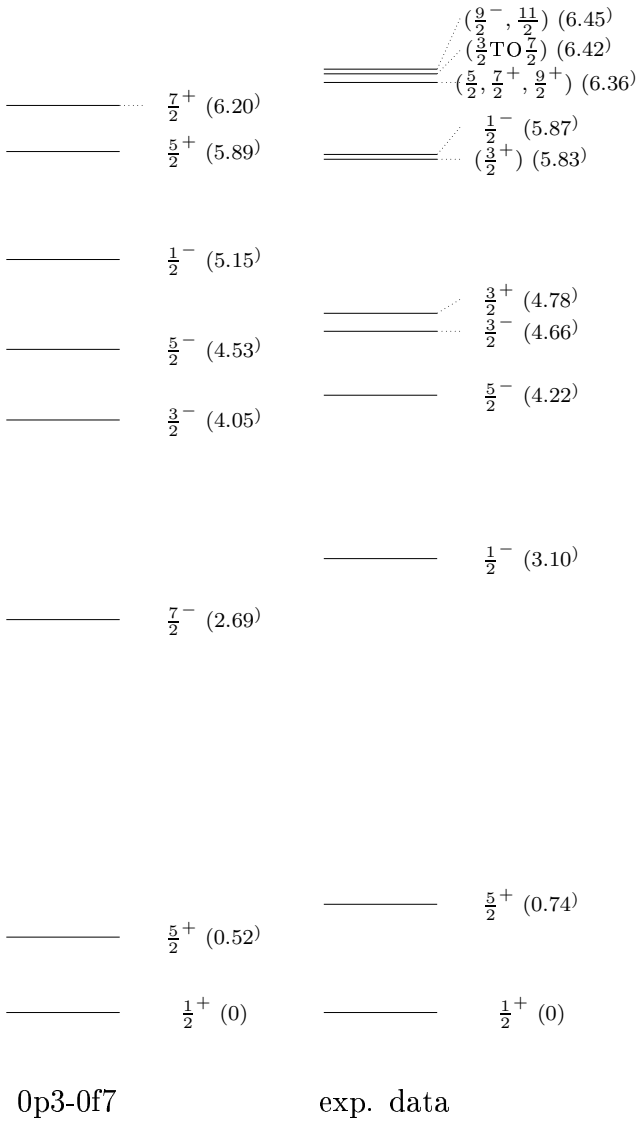

Figure 4.8: Energy spectra for 15C, in the reduced 0p3-0f7 model space. By reduced 0p3-0f7 model space we mean that we have reduced our 0p3-0f7 model space so that we have a maximum of 4 particles in the 0d5 orbital, a maximum of 2 particles in the 0d3 orbital and a maximum of 2 neutrons and 0 protons in the 0f7 orbital. The energies are given in MeV.

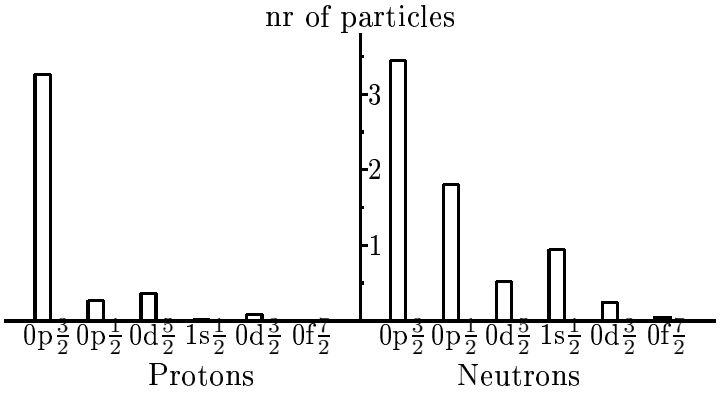

Figure 4.9: Orbital occupation for the ground state of ^{15}C with orbital momentum $J = \frac{1}{2}$, in the 0p3-0f7 model space.

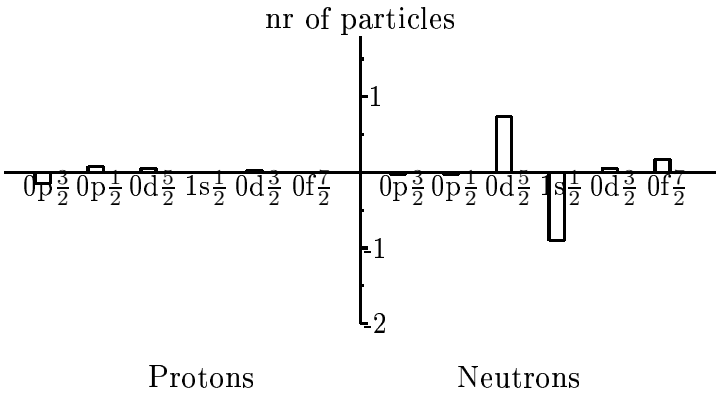

Figure 4.10: Orbital occupation difference from the ground state for the first $\frac{5}{2}^+$ state of ^{15}C, in the 0p3-0f7 model space.

Protons	$0p\frac{3}{2}$	$0p\frac{1}{2}$	$0d\frac{5}{2}$	$1s\frac{1}{2}$	$0d\frac{3}{2}$	$0f\frac{7}{2}$
Ground state $J = \frac{1}{2}^+$	3.26	0.27	0.37	0.02	0.09	0
First $\frac{5}{2}^+$ state	-0.15	+0.08	+0.05	0.00	+0.02	0
First $\frac{7}{2}^-$ state	-0.27	+0.12	+0.09	+0.01	+0.04	0
Second $\frac{3}{2}^-$ state	-0.29	+0.06	+0.15	+0.02	+0.05	0

Table 4.5: Proton orbital occupancy for ^{15}C in the $0p\frac{3}{2} - 0f\frac{7}{2}$ model space. The horizontal line gives the orbitals, and the vertical line gives the excited states. For the excited state the diagram shows the orbital occupancy difference from the ground state.

Neutrons	$0p\frac{3}{2}$	$0p\frac{1}{2}$	$0d\frac{5}{2}$	$1s\frac{1}{2}$	$0d\frac{3}{2}$	$0f\frac{7}{2}$
Ground state $J = \frac{1}{2}^+$	3.45	1.80	0.52	0.94	0.24	0.05
First $\frac{5}{2}^+$ state	-0.02	-0.03	+0.74	-0.90	+0.05	+0.17
First $\frac{7}{2}^-$ state	-0.05	-0.07	+0.45	-0.90	+0.09	+0.48
Second $\frac{3}{2}^-$ state	-0.36	-0.11	+0.51	-0.26	+0.14	+0.08

Table 4.6: Neutron orbital occupancy for ^{15}C in the $0p\frac{3}{2} - 0f\frac{7}{2}$ model space. The horizontal line gives the orbitals, and the vertical line gives the excited states. For the excited state the diagram shows the orbital occupancy difference from the ground state.

4.3 ^{15}B

For ^{15}B we have much the same situation as for ^{15}C, with a nucleus dominated by neutron excitations from the $1s\frac{1}{2}$ orbital to the $0d\frac{5}{2}$ orbital (see figure 4.15 and tables **??**-4.10). We also get a good correspondence between our calculated states in the $0p\frac{3}{2} - 0f\frac{7}{2}$ model space and the experimental states.

It will be interesting to see if ^{16}C also follows the expectations previously held about its excitations, or if it is ruled by other types of excitations that supports the experimental data on ^{16}C from the Imai et al. [1] experiment.

4.3.1 $0p\frac{3}{2} - 0d\frac{3}{2}$ model space

Figure 4.11 shows the energy spectra for ^{15}B. Looking at the spectrum for $0p\frac{3}{2} - 0d\frac{3}{2}$ model space we see that we predict both of the experimental values, but we have a much higher energy on our states, the first excited state being over 50% larger than the corresponding experimental state. We also predict a $\frac{3}{2}^-$ state above the $\frac{7}{2}^-$ state.

Figure 4.12 shows the ground state occupancy of ^{15}B in the $0p\frac{3}{2} - 0d\frac{3}{2}$ model space. The ground state is very similar to the ground state of ^{15}C, but with only 3 protons in the $0p\frac{3}{2}$ orbital and one neutron more that spreads out among all the available orbitals.

Figure 4.13 shows the sp orbitals occupancy of the excited states of ^{15}B in the $0p\frac{3}{2} - 0d\frac{3}{2}$ model space. We see that we have almost exclusively neutron excitations from the $1s\frac{1}{2}$ orbital to the $0d\frac{5}{2}$ orbital.

4.3.2 $0p\frac{3}{2} - 0f\frac{7}{2}$ model space

We now take for us the $0p\frac{3}{2} - 0f\frac{7}{2}$ model space energy spectrum of ^{15}B in figure 4.11. The excited states are now much closer to their corresponding experimental values.

The ground state (see figure 4.14) has now an equal amount of neutrons (roughly 1 neutron) in the $0d\frac{5}{2}$ and $1s\frac{1}{2}$ orbitals. Otherwise it is the same as for the $0p\frac{3}{2} - 0d\frac{3}{2}$ model space.

The $\frac{5}{2}^-$ state now lies 0.13 MeV (10.1%) above the corresponding experimental state. The $\frac{7}{2}^-$ state lies 0.47 MeV (17.0%) above the corresponding experimental state. These states now have a considerably lower amount of neutrons being excited from the $1s\frac{1}{2}$ orbital to the $0d\frac{5}{2}$ orbital.

The third excited state we predict has changed from being a $\frac{3}{2}^-$ state to being a $\frac{1}{2}^-$ state. This state has an excitation energy of 4.32 MeV. The state has, in addition to a one neutron excitation from the $1s\frac{1}{2}$ orbital to the $0d\frac{3}{2}$ orbital, small proton excitations from the $0p\frac{3}{2}$ orbital to the $0p\frac{1}{2}$ orbital and small neutron excitations from the $1s\frac{1}{2}$ orbital to the $0f\frac{7}{2}$ orbital

We predict the two experimental states which have been obtained, though we get too high energy for our states. The excited states are ruled by neutron excitations from the $1s\frac{1}{2}$ orbital to the $0d\frac{5}{2}$ orbital, in correspondence with our expectations.

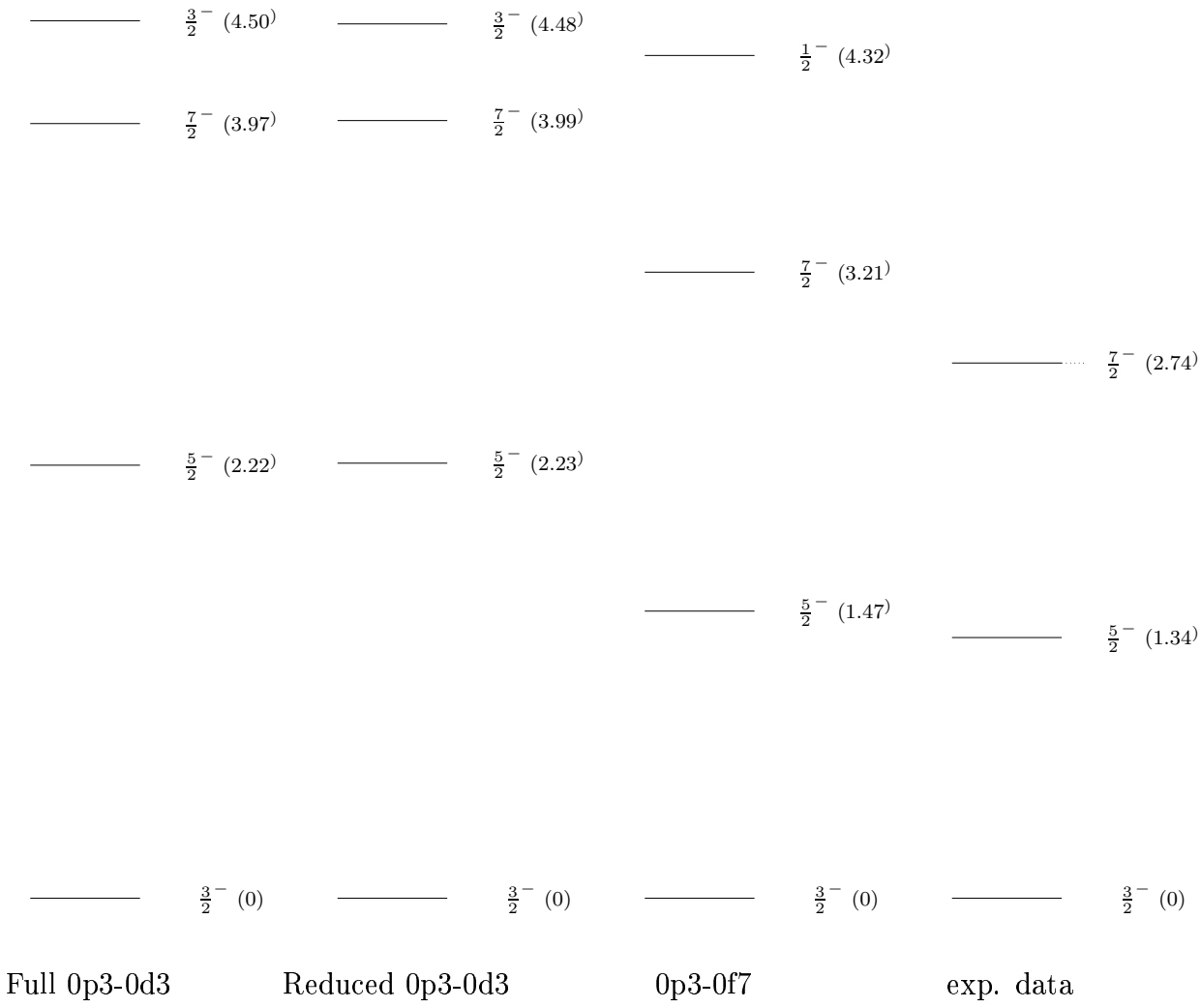

Figure 4.11: Energy spectra for 15B, in the full 0p3-0d3 and reduced 0p3-0f7 model spaces. Reduced 0p3-0d3 means that we have reduced our 0p3-0d3 model space so that we have a maximum of 4 particles in the 0d5 orbital and a maximum of 2 particles in the 0d3 orbital. Reduced 0p3-0f7 model space we mean that we have reduced our 0p3-0f7 model space so that we have a maximum of 4 particles in the 0d5 orbital, a maximum of 2 particles in the 0d3 orbital and a maximum of 2 particles in the 0f7 orbital. The energies are given in MeV.

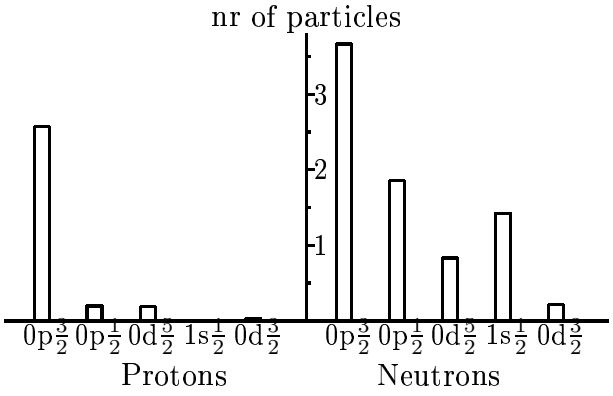

Figure 4.12: Orbital occupation for the ground state of ^{15}B with orbital momentum $J = \frac{3}{2}^-$, in the 0p3-0d3 model space.

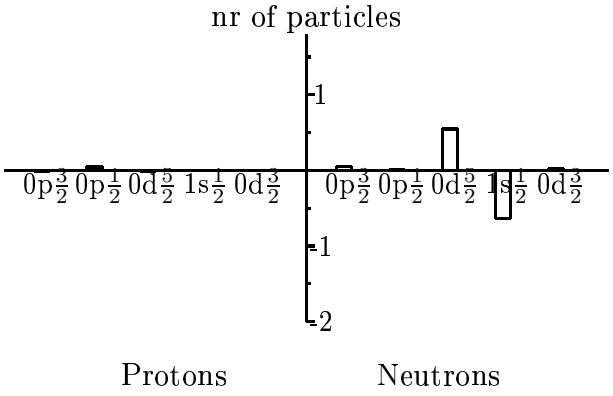

Figure 4.13: Orbital occupation difference from the ground state for the first $\frac{5}{2}^-$ state of ^{15}B, in the 0p3-0d3 model space.

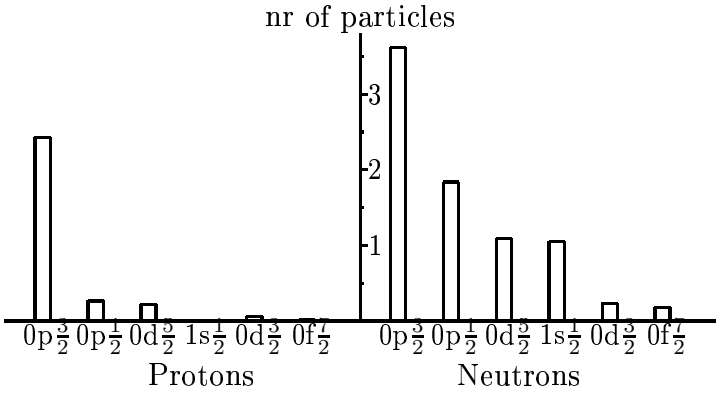

Figure 4.14: Orbital occupation for the ground state of ^{15}B with orbital momentum $J = \frac{3}{2}^-$, in the 0p3-0f7 model space.

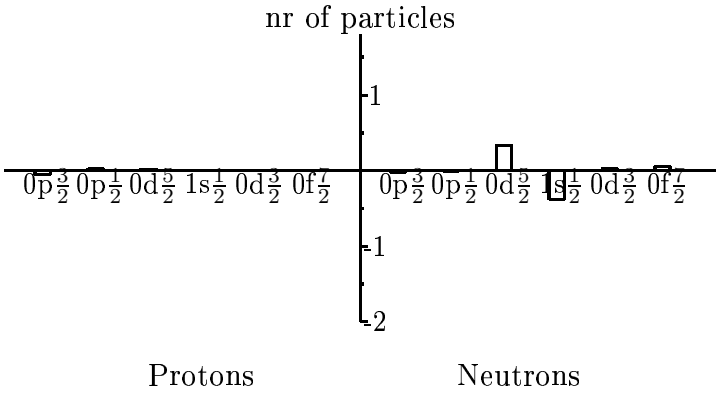

Figure 4.15: Orbital occupation difference from the ground state for the first $\frac{5}{2}^-$ state of ^{15}B, in the 0p3-0f7 model space.

Protons	$0p\frac{3}{2}$	$0p\frac{1}{2}$	$0d\frac{5}{2}$	$1s\frac{1}{2}$	$0d\frac{3}{2}$
Ground state $J = \frac{3}{2}^-$	2.57	0.20	0.19	0.01	0.03
First $\frac{5}{2}^-$ state	-0.02	+0.04	-0.02	0.00	0.00
First $\frac{7}{2}^-$ state	-0.01	+0.01	0.00	0.00	0.00
Second $\frac{3}{2}^-$ state	-0.02	+0.01	+0.01	0.00	0.00

Table 4.7: Proton orbital occupancy for ^{15}B in the $0p\frac{3}{2} - 0d\frac{3}{2}$ model space. The horizontal line gives the orbitals, and the vertical line gives the excited states. For the excited state the diagram shows the orbital occupancy difference from the ground state.

Neutrons	$0p\frac{3}{2}$	$0p\frac{1}{2}$	$0d\frac{5}{2}$	$1s\frac{1}{2}$	$0d\frac{3}{2}$
Ground state $J = \frac{3}{2}^-$	3.66	1.86	0.83	1.43	0.22
First $\frac{5}{2}^-$ state	+0.06	+0.01	+0.55	-0.64	+0.02
First $\frac{7}{2}^-$ state	+0.03	+0.01	+0.60	-0.67	+0.03
Second $\frac{3}{2}^-$ state	+0.01	-0.01	+0.30	-0.28	0.00

Table 4.8: Neutron orbital occupancy for ^{15}B in the $0p\frac{3}{2} - 0d\frac{3}{2}$ model space. The horizontal line gives the orbitals, and the vertical line gives the excited states. For the excited state the diagram shows the orbital occupancy difference from the ground state.

Protons	$0p\frac{3}{2}$	$0p\frac{1}{2}$	$0d\frac{5}{2}$	$1s\frac{1}{2}$	$0d\frac{3}{2}$	$0f\frac{7}{2}$
Ground state $J = \frac{3}{2}^-$	2.43	0.26	0.22	0.01	0.06	0.02
First $\frac{5}{2}^-$ state	-0.05	+0.03	+0.02	0.00	0.00	0.00
First $\frac{7}{2}^-$ state	-0.05	0.00	+0.04	0.00	0.00	0.00
Second $\frac{3}{2}^-$ state	-0.24	+0.16	+0.06	+0.01	+0.02	0.00

Table 4.9: Proton orbital occupancy for ^{15}B in the $0p\frac{3}{2} - 0f\frac{7}{2}$ model space. The horizontal line gives the orbitals, and the vertical line gives the excited states. For the excited state the diagram shows the orbital occupancy difference from the ground state.

Neutrons	$0p\frac{3}{2}$	$0p\frac{1}{2}$	$0d\frac{5}{2}$	$1s\frac{1}{2}$	$0d\frac{3}{2}$	$0f\frac{7}{2}$
Ground state $J = \frac{3}{2}^-$	3.62	1.84	1.09	1.05	0.23	0.17
First $\frac{5}{2}^-$ state	-0.02	-0.02	+0.33	-0.38	+0.03	+0.05
First $\frac{7}{2}^-$ state	-0.06	-0.03	+0.45	-0.51	+0.06	+0.07
Second $\frac{3}{2}^-$ state	-0.06	-0.06	+0.69	-0.87	+0.06	+0.24

Table 4.10: Neutron orbital occupancy for ^{15}B in the $0p\frac{3}{2} - 0f\frac{7}{2}$ model space. The horizontal line gives the orbitals, and the vertical line gives the excited states. For the excited state the diagram shows the orbital occupancy difference from the ground state.

4.4 ^{16}C

In ^{16}C we have again mostly one-neutron excitations from the $1s\frac{1}{2}$ orbital to the $0d\frac{5}{2}$ orbital, similar to what we have seen in ^{15}C and ^{15}B, see figure 4.20 and tables **??-??**. We also have a very good correspondence between our predicted states in the $0p\frac{3}{2}-0f\frac{7}{2}$ model space and the experimental states.

4.4.1 $0p\frac{3}{2}-0d\frac{3}{2}$ model space

Figure 4.16 shows the energy spectra for ^{16}C in the $0p\frac{3}{2}-0d\frac{3}{2}$ model space. We notice that the excited states have a much higher energy than the experimental states, our first excited state having almost twice the energy of the corresponding experimental state.

Figures 4.17 - 4.18 show the sp orbital occupancy of ^{16}C in the $0p\frac{3}{2}-0d\frac{3}{2}$ model space. The ground state has roughly two neutrons more in the $1s\frac{1}{2}$ orbital than ^{14}C, and has otherwise almost the same orbital occupancy. The excited states of ^{16}C are essentially dominated by neutron excitations from the $1s\frac{1}{2}$ orbital to the $0d\frac{5}{2}$ orbital. This shows that for ^{16}C, the $0d\frac{5}{2}$ orbital has a higher excitation energy than the $1s\frac{1}{2}$ orbital.

4.4.2 $0p\frac{3}{2}-0f\frac{7}{2}$ model space

Figure 4.16 shows the sp orbital occupancy of ^{16}C in the $0p\frac{3}{2}-0f\frac{7}{2}$ model space. The energy spectrum given here is in much better agreement with the experimental data. The three excited states calculated appear in the correct order. The first 2^+ state corresponds well with the experimental value, and the second 2^+ state and first 0^+ state corresponds very well with the experimental data

Figures 4.19 - 4.20 show the sp orbital occupancy of ^{16}C in the $0p\frac{3}{2}-0f\frac{7}{2}$ model space. The ground state has roughly one neutron more in the $0d\frac{5}{2}$ orbital and one neutron less in the $1s\frac{1}{2}$ orbital when compared with the ground state for ^{16}C in the $0p\frac{3}{2}-0d\frac{3}{2}$ model space. When compared to the ground state for ^{15}C in the $0p\frac{3}{2}-0f\frac{7}{2}$ model space, we have roughly one neutron more in the $0d\frac{5}{2}$ orbital. This follows our predictions. It is interesting, however, that the inclusion of the $0f7$ orbital moves one particle from the $1s\frac{1}{2}$ orbital to the $0d\frac{5}{2}$ orbital.

Our first 2^+ state has an energy difference with the corresponding experimental state of 6.2%. It consists mainly of neutron excitations from the $1s\frac{1}{2}$ orbital to the $0d\frac{5}{2}$ orbital, but with roughly half as many neutrons as the same state in the $0p\frac{3}{2}-0d\frac{3}{2}$ model space.

The first 0^+ state has an energy difference with the corresponding experimental state of only 0.06%.

The second 2^+ state has an energy difference with the corresponding experimental state of 1.5%. The protons play a larger role here, with a low amount of protons being

excited from the $0p\frac{3}{2}$ orbital to mostly the $0p\frac{1}{2}$ orbital. We again have a relatively large amount of neutrons being excited from the $1s\frac{1}{2}$ orbital, to the $0d\frac{5}{2}$ and $0f\frac{7}{2}$ orbitals, with most of the neutrons going to the $0d\frac{5}{2}$ orbital, in accordance with theory.

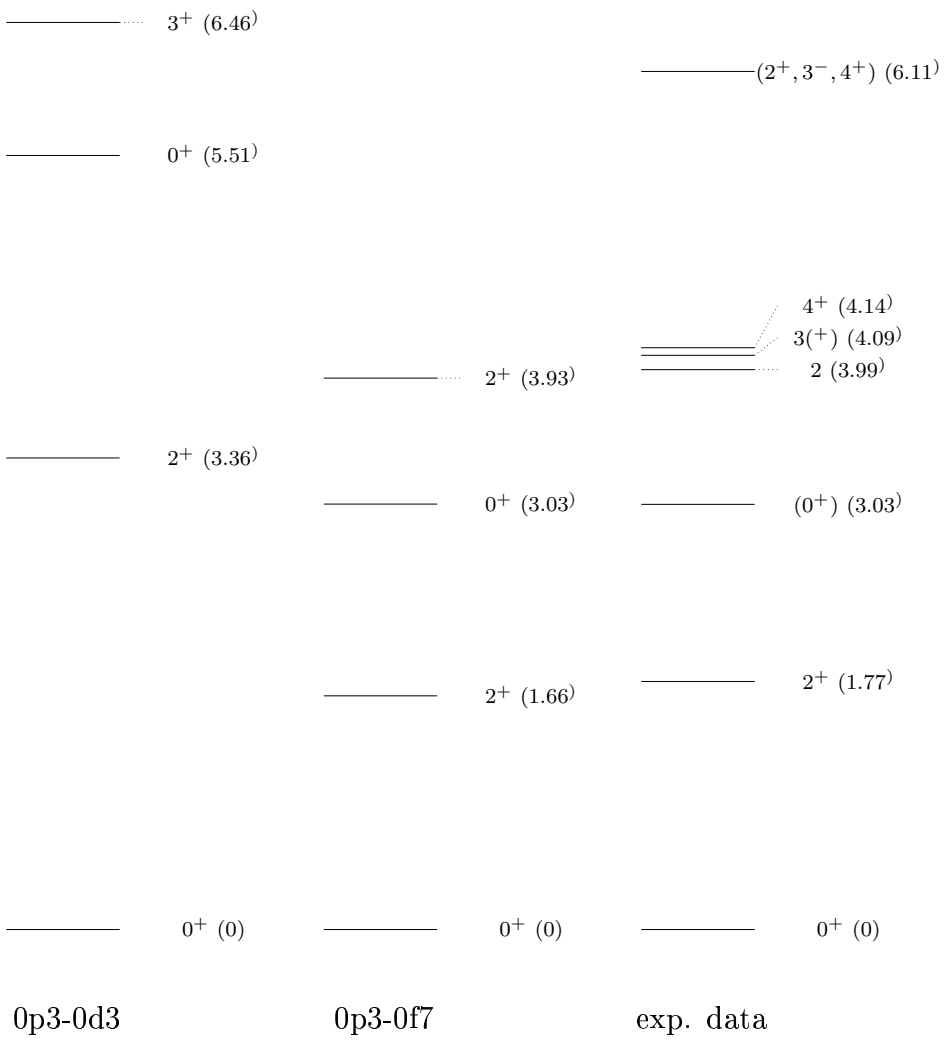

Figure 4.16: Energy spectra for 16C, in the full 0p3-0d3 and reduced 0p3-0f7 model spaces. By reduced 0p3-0f7 model space we mean that we have reduced our 0p3-0f7 model space so that we have a maximum of 4 particles in the 0d5 orbital, a maximum of 2 particles in the 0d3 orbital and maximum of 2 neutrons and 0 protons in the 0f7 orbital. The energies are given in MeV.

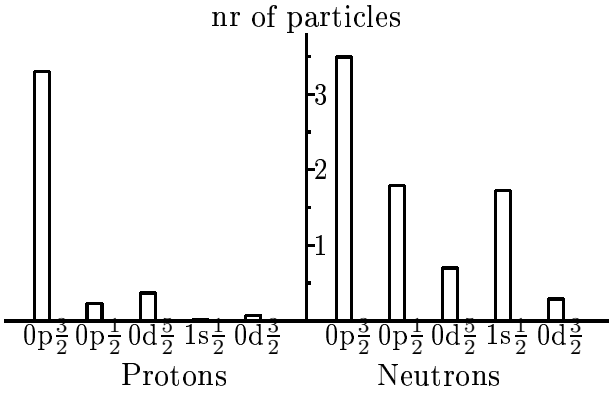

Figure 4.17: Orbital occupation for the ground state of ^{16}C with orbital momentum $J = 0^+$, in the 0p3-0d3 model space.

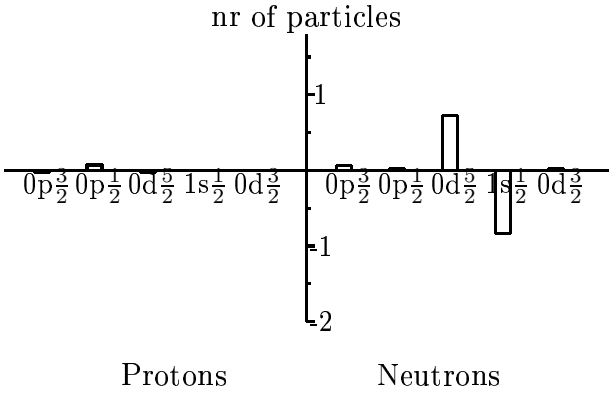

Figure 4.18: Orbital occupation difference from the ground state for the first 2^+ state of ^{16}C, in the 0p3-0d3 model space.

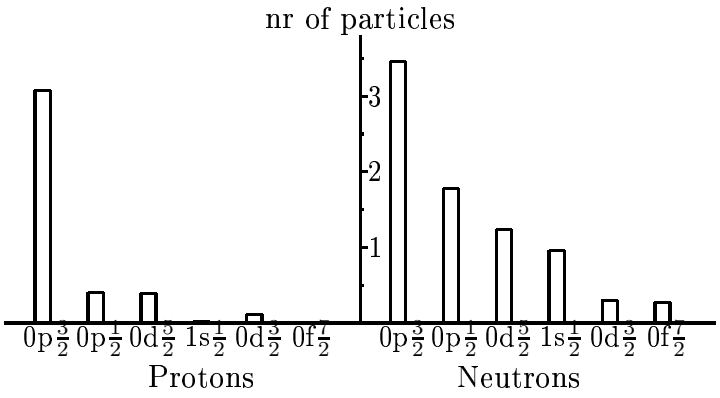

Figure 4.19: Orbital occupation for the ground state of ^{16}C with orbital momentum $J = 0^+$, in the 0p3-0f7 model space.

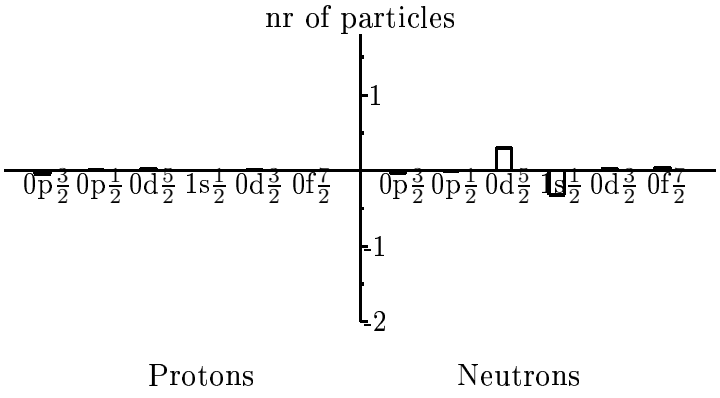

Figure 4.20: Orbital occupation difference from the ground state for the first 2^+ state of ^{16}C, in the 0p3-0f7 model space.

Protons	$0p\frac{3}{2}$	$0p\frac{1}{2}$	$0d\frac{5}{2}$	$1s\frac{1}{2}$	$0d\frac{3}{2}$
Ground state $J = 0^+$	3.30	0.24	0.37	0.02	0.08
First 2^+ state	-0.03	+0.07	-0.03	0.00	0.00
First 0^+ state	-0.06	+0.11	-0.04	0.00	-0.01
Second 3^+ state	+0.02	+0.03	-0.03	0.00	-0.01

Table 4.11: Proton orbital occupancy for ^{16}C in the $0p\frac{3}{2} - 0d\frac{3}{2}$ model space. The horizontal line gives the orbitals, and the vertical line gives the excited states. For the excited state the diagram shows the orbital occupancy difference from the ground state.

Neutrons	$0p\frac{3}{2}$	$0p\frac{1}{2}$	$0d\frac{5}{2}$	$1s\frac{1}{2}$	$0d\frac{3}{2}$
Ground state $J = 0^+$	3.49	1.79	0.70	1.73	0.29
First 2^+ state	+0.06	+0.02	+0.74	-0.84	+0.03
First 0^+ state	+0.03	+0.02	+1.42	-1.50	+0.03
Second 3^+ state	+0.08	+0.02	+0.69	-0.76	-0.04

Table 4.12: Neutron orbital occupancy for ^{16}C in the $0p\frac{3}{2} - 0d\frac{3}{2}$ model space. The horizontal line gives the orbitals, and the vertical line gives the excited states. For the excited state the diagram shows the orbital occupancy difference from the ground state.

Protons	$0p\frac{3}{2}$	$0p\frac{1}{2}$	$0d\frac{5}{2}$	$1s\frac{1}{2}$	$0d\frac{3}{2}$	$0f\frac{7}{2}$
Ground state $J = 0^+$	3.08	0.40	0.39	0.02	0.11	0
First 2^+ state	-0.04	+0.01	+0.02	0.00	+0.01	0
First 0^+ state	-0.03	+0.04	-0.01	0.00	+0.01	0
Second 2^+ state	-0.20	+0.14	+0.03	+0.01	+0.03	0

Table 4.13: Proton orbital occupancy for ^{16}C in the $0p\frac{3}{2} - 0f\frac{7}{2}$ model space. The horizontal line gives the orbitals, and the vertical line gives the excited states. For the excited state the diagram shows the orbital occupancy difference from the ground state.

Neutrons	$0p\frac{3}{2}$	$0p\frac{1}{2}$	$0d\frac{5}{2}$	$1s\frac{1}{2}$	$0d\frac{3}{2}$	$0f\frac{7}{2}$
Ground state $J = 0^+$	3.46	1.78	1.23	0.96	0.30	0.27
First 2^+ state	-0.03	-0.02	+0.30	-0.32	+0.03	+0.04
First 0^+ state	+0.04	+0.01	-0.03	-0.03	-0.01	+0.03
Second 2^+ state	0.00	-0.03	+0.43	-0.62	+0.03	+0.20

Table 4.14: Neutron orbital occupancy for ^{16}C in the $0p\frac{3}{2} - 0f\frac{7}{2}$ model space. The horizontal line gives the orbitals, and the vertical line gives the excited states. For the excited state the diagram shows the orbital occupancy difference from the ground state.

4.5 Final notes about the energy spectra

Concerning the orbital occupancies, we see that going to the $0p\frac{3}{2} - 0f\frac{7}{2}$ model space we have, in general, excitations from and to the same orbitals that we had in the $0p\frac{3}{2} - 0d\frac{3}{2}$ model space, but often with a lower amount of particles being excited. The energy values of our excited states in the $0p\frac{3}{2} - 0d\frac{3}{2}$ model space are, for the most part, too high, lying typically 1-2 MeV above the experimental states. Including the $0p\frac{3}{2} - 0f\frac{7}{2}$ model space brings this energy down to being 0.01-0.8 MeV away from from the experimental states.

The orbital occupations of the ground state of ^{15}B and ^{16}C are very similar. The orbital occupations for the excited states are also similar to each other. This is as expected, as the two nuclei have the same number of neutrons, and the only difference between the them is one proton in the $0p\frac{1}{2}$ orbital.

Notice that when we have six free neutrons (^{14}C and ^{16}O) the ground state will have between 0.5 and 1 neutrons in the $0d$ shell instead of the $0p$ shell. And when we have eight free neutrons (^{16}C and ^{15}B) we generally have more neutrons in the $1s\frac{1}{2}$ orbital than in the $0d\frac{5}{2}$ orbital. When the nucleus is excited, particles in the $1s\frac{1}{2}$ orbital are excited to the $0d\frac{5}{2}$ orbital. This shows that, as there begins to be more than one particle in the in the $0d\frac{5}{2}$ orbital, the $1s\frac{1}{2}$ orbital becomes more energetically favorable to excite to than the $0d\frac{5}{2}$ orbital.

4.6 E2 Transitions

The transition strength of ^{14}C is, as was mentioned in the introduction, $3.7e^2\text{fm}^4$ [1]. For ^{16}C the transition strength is $4.15e^2\text{fm}^4$ [2].

To find the transition strength I need to specify the effective neutron and proton charges. These charges need to reflect the constraints we have on our model space, and are typically chosen as $1.0 - 1.5$. However, since we have such a large model space, then our effective charges should be much closer to the real charges of 0 and 1 for the neutron and proton, respectively.

Figure 4.21 shows a 3-D plot of the transition strength for ^{14}C as a function of the neutron and proton charges, marked in red. The experimental value is plotted in green. Figure 4.22 shows the neutron and proton charges for ^{16}C that gives us the experimental value of the transition strength at $0.474e^2\text{fm}^4$. The neutron charge goes from $0.1 - 0.5$, and the proton charge goes from $1.0 - 1.4$. The values are discussed below.

4.6.1 ^{14}C

For ^{14}C we see that our data does not correspond so well with the experimental value of $0.423e^2\text{fm}^4$. We see that the transition strength increases when we increase the proton or neutron charge, and it is lowest when we have an effective charge of 0.1 for

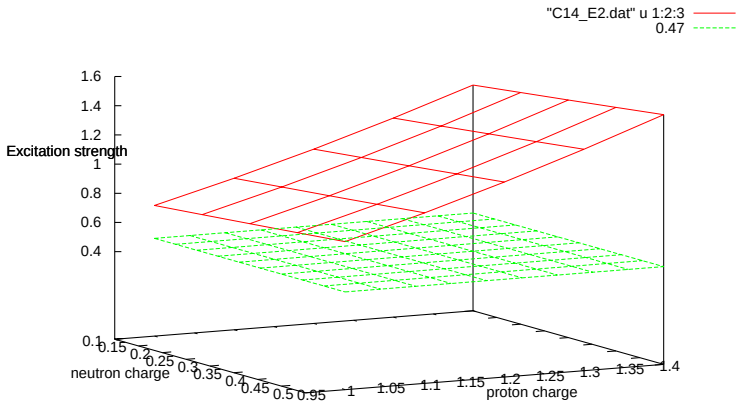

Figure 4.21: Transition strength for ^{14}C as a function of proton and neutron effective charge. The red field shows the calculated transition strength, while the green field shows the experimental transition strength. The important thing to notice here is that the red field never crosses the green field, and the red field decreases with the proton and neutron charge.

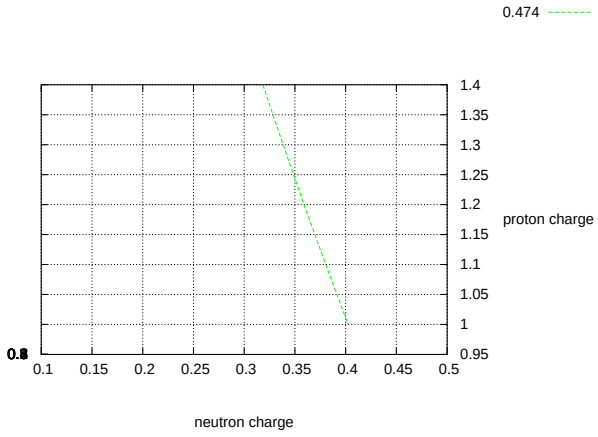

Figure 4.22: The effective neutron and proton charges for ^{16}C that correspond to the experimental transition strength at $0.474e^2\text{fm}^4$.

the neutron and 1.0 for the proton. The transition strength is also more dependent on the proton charge than on the neutron charge. For an effective charge of 0 for the neutron and 1 for the proton we get a transition strength of $0.667e^2\text{fm}^4$. This is 1.5 times the experimental value. This high value indicates that the E2 transition for ^{14}C is complicated, and cannot be accurately described by our model. There are mainly three effects, in addition to the model space factor, that we have not taken into account that might be strongly involved in the transition. One is the resonances in ^{14}C. The other is center-of-mass corrections, the third is three-body interactions. As ^{14}C has many resonant states, I expect this to be the main contributor to the transition strength of these three effect.
!Er ikke sikker paa den siste setningen her, eller paa hvor stor innvirkning disse effektene kan ha for overgangsstyrken.!
Although we could not predict the transition strength, the high proton charge dependency is in accordance with our previous observations of the orbital occupancy of ^{14}C.

4.6.2 ^{16}C

For ^{16}C our data corresponds well with the experimental value of $0.474e^2\text{fm}^4$. A good choice for the effective charges would be to set the proton charge to 1.0, as this value is closest to the real charge of the proton, and because the E2 transition for ^{16}C is mostly dependent upon the neutron charge. For a proton charge of 1.0, the neutron charge 1.4 gives us the transition strength $.470e^2\text{fm}^4$, which corresponds very well with the experimental value. That the transition is ruled by the neutron charge is in accordance with our previous observations of the orbital occupancy of ^{16}C.

Chapter 5

Conclusion

The goal of this thesis was to see if we could predict the $E2_1^+$ transition strength for ^{16}C that was measured by the authors of Ref. [1]. This experimental result would have indicated that the physics of the low-lying states would have been dominated by collective proton-neutron excitations. New experiments corrected however this value by almost one order of magnitude. Our theoretical results are in line with the revised experimental results and do not predict any new physics involving the nuclei ^{14}C, ^{15}C, ^{15}B and ^{16}C.

We could however not predict the $E2_1^+$ transition strength of ^{14}C. This may suggest that this transition is more complex than we have taken into account for.

An important part in the calculations has been to not adjust the effective interaction. We wanted to study the role played by different model spaces and computed therefore effective interactions taylored to each specific model space. We have however used single particle (sp) energies that have been adjusted to ^{16}O, but have not done any further adjustments on these sp energies.

We have seen that we reproduce rather well most of the low-lying states, though the energy values sometimes are too high. For all the nuclei we reproduce the first excited. For ^{14}C and ^{15}C we need to work more on the effective interaction and the size of the model space. The nuclei ^{15}B and ^{16}C, on the otherhand, come out well.

We have seen that the $0p\frac{3}{2} - 0f\frac{7}{2}$ model space gives a better reproduction of the experimental values when compared to the $0p\frac{3}{2} - 0d\frac{3}{2}$ model space. In some cases (see ^{16}C, figure 4.16) we obtain a very good agreement with the experimental states. It should also be noted that we have only calculated a few of the states for each nucleus, and it is therefore difficult to draw a conclusion on how much of an improvement the $0p\frac{3}{2} - 0f\frac{7}{2}$ model space is. To further test the effect of higher-lying single-particle states, we would need to include degrees of freedom from the $1p_{3/2}$ orbit and eventually from the $1p_{1/2}$ and $0f_{5/2}$ single particle orbitals. With the new parallel version of the shell-model code this can be tested soon.

Though there are several states, mostly in ^{14}C, that we have not reproduced and though the excitation energy sometimes is significantly higher than the experimental

value, there are several important aspects of studied the nuclei that we have been able to describe.

We have seen that ^{14}C is mostly dominated by proton excitations, while ^{15}C, ^{15}B and ^{16}C are mostly dominated by neutron excitations. We have also seen that for ^{15}C the $0d\frac{5}{2}$ orbital has higher energy than the $1s\frac{1}{2}$ orbital. All of these are in agreement with experimental findings.

There are still several things that can be improved in our effective interaction. I will list these here. The first three requires additional code to be written for the program we have used, while the fourth implies a larger Hamiltonian matrix to diagonalize.

- Resonances. They are important for ^{14}C, as previously discussed, and would most likely improve our results for this nucleus.
- Removal of spurious center of mass corrections. This is another correction that probably could improve our results, in particular for negative parity would give.
- Three-particle interactions arising from effective three-nucleon interactions and eventually from three-body forces. These are important corrections, although they tend to effect mainly the ground state energies.
- Size of model space. Increasing our model-space is an obvious improvement. However, this is restricted by computational power and would require better algorithms or more powerful computers with more storage capasity. Still, it would be a good improvement, as we could then see if we have a convergence in our states. There are two ways to improve our model space. One is to increase the number of particles we allow in the high-lying orbitals, such as the $0f\frac{7}{2}$ orbital, which would be an improvement for high-lying states. For the low-lying states we have looked at, it is doubtful that it would bring any significant change to our states. However, it is worth studying if our restrictions on the $0p\frac{3}{2} - 0f\frac{7}{2}$ model-space are good, especially the exclusion of protons from the $0f\frac{7}{2}$ orbital, which I have only looked at qualitatively. Another, more important improvement, would be to increase our model-space by including the $1p\frac{3}{2}$, $1p\frac{1}{2}$ and $0f_{5/2}$ single-particle orbitals.

Bibliography

[1] N. Imai, H. J. Ong, N. Aoi, H. Sakurai, K. Demichi, H. Kawasaki, H. Baba, Zs. Dombrádi, Z. Elekes, N. Fukuda, Zs. Fülöp, A. Gelberg, T. Gomi, H. Hasegawa, K. Ishikawa, H. Iwasaki, E. Kaneko, S. Kanno, T. Kishida, Y. Kondo, T. Kubo, K. Kurita, S. Michimasa, T. Minemura, M. Miura, T. Motobayashi, and T. Nakamura. Anomalously hindered e2 strength b(e2;$2_1^+ \rightarrow 0_1^+$) in ^{16}c. *Phys. Rev. Lett.*, 92:062501, Feb 2004.

[2] M. Wiedeking, P. Fallon, A. O. Macchiavelli, J. Gibelin, M. S. Basunia, R. M. Clark, M. Cromaz, M.-A. Deleplanque, S. Gros, H. B. Jeppesen, P. T. Lake, I.-Y. Lee, L. G. Moretto, J. Pavan, L. Phair, E. Rodriguez-Vietiez, L. A. Bernstein, D. L. Bleuel, J. T. Burke, S. R. Lesher, B. F. Lyles, and N. D. Scielzo. Lifetime measurement of the first excited 2^+ state in ^{1}6c. *Physical Review Letters*, 65: 152501, 2008.

[3] E. K. Warburton and B. A. Brown. Effective interactions for the 0p1s0d nuclear shell-model space. *Physical Review C*, 46:923, 1992.

[4] Eivind Osnes M. Hjorth-Jensen, Thomas T.S. Kuo. Realistic effective interactions for nuclear systems. *Phys Reports*, 261:125, 1995.

[5] M. Hjorth-Jensen D.J. Dean, G. Hagen and T. Papenbrock. Effective interactions and coupled cluster theories for stable and unstable nuclei. 2007.

[6] T.T.S. Kuo. Topics in many-body theory of nuclear effective interactions. *Lecture Notes in Physics*, 144:248, 1981.

[7] K.A. Brueckner. *Phys. Rev.*, 97:1353, 1955.

[8] J. Goldstone. *Proc. Roy. Soc. A*, 293:267, 1957.

[9] B.H. Brandow H.A. Bethe and A.G. Petschek. *Phys. Rev.*, 129:225, 1963.

[10] S. Fujii, E. Epelbaum, H. Kamada, R. Okamoto, K. Suzuki, and W. Glöckle. Low-momentum nucleon-nucleon interaction and its application to few-nucleon systems. *Phys. Rev. C*, 70:024003, Aug 2004.

[11] O. Heinonen E.K.U. Gross, E. Runge. *Many - particle theory.* 1991.

[12] Håvar Bentsen. Kjerne strukturberegninger for kalsium. hovedoppgave i kjernefysikk. 1995.

[13] B.J. Cole R.R. Whitehead, A. Watt and I. Morrison. *Adv. in Nucl. Phys.*, 9:123, 1977.

[14] E.R. Davidson. *Computers in Physics*, 7:519, 1993.

[15] Brussaard and Glaudemans. *Nuclear Shell Theory.* North-Holland Publishing Company, 1977.

[16] National nuclear data center. URL `http://www.nndc.bnl.gov/`.